

Proteomic analysis identifies the E3 ubiquitin ligase Pdzrn3 as a regulatory target of Wnt5a-Ror signaling

Sara E. Konopelski¹, Michael W. Susman², Ryan C. Kunz³, Jia Tan¹, Michael D. Cohen¹, Kyoko Okada¹, Helen Lamb¹, Shannon S. Choi¹, Edith P. Karuna¹, Michael K. Scales¹, Steven P. Gygi³, Michael E. Greenberg², and Hsin-Yi Henry Ho^{1,2,*}

¹Department of Cell Biology and Human Anatomy, University of California Davis, School of Medicine, Davis, CA, USA

²Department of Neurobiology, Harvard Medical School, Boston, MA, USA

³Department of Cell Biology, Harvard Medical School, Boston, MA, USA

*For correspondence: hyhho@ucdavis.edu

Abstract

Wnt5a-Ror signaling is a conserved pathway that regulates morphogenetic processes during vertebrate development, but its downstream signaling events remain poorly understood. By conducting a large-scale proteomic screen in mouse embryonic fibroblasts, we identified the E3 ubiquitin ligase Pdzrn3 as a new regulatory target that is degraded upon pathway activation in a β -catenin-independent, ubiquitin-proteasome system-dependent manner. We developed a flow cytometry-based reporter to monitor Pdzrn3 abundance and delineated a signaling cascade involving Frizzled, Dishevelled, Casein kinase 1, and Glycogen synthase kinase 3 that regulates Pdzrn3 stability. Genetic epistasis analysis suggests that Pdzrn3 degradation occurs downstream of Dishevelled but independently of Kif26b, a previously identified Wnt5a-Ror-Dishevelled signaling target. Further, we discovered that Pdzrn3 degradation requires Wnt5a-dependent phosphorylation of three residues within its C-terminal LNX3H domain, which is conserved in other homologs and likely functions as a Wnt5a-responsive domain. Collectively, this work establishes a new Wnt5a-Ror signaling cascade involving Pdzrn3 phosphorylation and degradation.

Introduction

Embryonic development in vertebrates is a highly stereotyped and coordinated process that depends on a handful of core signaling pathways. One major mode of signaling involves Wnt ligands, a diverse and highly conserved family of glycoproteins that signal in many spatiotemporal contexts, including tissue specification and tissue morphogenesis in addition to tissue homeostasis in adult organisms (Clevers and Nusse, 2012, Nusse and Varmus, 2012, Steinhart and Angers, 2018). Thus, Wnts play unique and critical roles in both developing and adult organisms.

Traditionally, Wnt pathways have been classified as either canonical or non-canonical. Canonical Wnt signaling utilizes β -catenin as a transcriptional co-activator to regulate cell fate and proliferation and is relatively well understood. In contrast, non-canonical Wnt signaling, which regulates tissue morphogenetic processes in a β -catenin independent manner, remains poorly characterized (Clevers and Nusse, 2012, Nusse and Varmus, 2012, Steinhart and Angers, 2018, Veeman et al., 2003). Numerous studies in a variety of model organisms have demonstrated that alterations to the expression of Wnt5a, the prototypic non-canonical Wnt ligand, can cause drastic morphogenesis defects such as body axis truncations, shortened limbs and tails, and many craniofacial malformations (Moon et al., 1993, Yamaguchi et al., 1999, Hikasa et al., 2002). These phenotypic abnormalities closely mirror those of Ror1 and Ror2 double knockout mice, further underscoring the growing evidence that Ror receptors mediate Wnt5a signals to orchestrate tissue morphogenetic events (Nomi et al., 2001, Ho et al., 2012).

Importantly, the phenotypic characteristics observed in *WNT5A* and *ROR2* mutants, namely body axis and limb truncations and craniofacial malformations, have also been observed in human Robinow syndrome patients, and several recent publications indicate that numerous Robinow syndrome patients possess mutations in various components of Wnt5a-Ror signaling, including *WNT5A*, *ROR2*, *FRIZZLED2* (*FZD2*), *DISHEVELLED1* (*DVL1*), and *DISHEVELLED3* (*DVL3*) (Afzal et al., 2000, Afzal and Jeffery, 2003, Person et al., 2010, Bunn et al., 2015, White et al., 2015, White et al., 2016, White et al., 2018). Further, bulldogs and other closely related dog breeds possess an analogous frameshift mutation in *DISHEVELLED2* (*DVL2*) and exhibit highly similar craniofacial and skeletal features (Mansour et al., 2018). Collectively, these recent findings strongly support the idea that Wnt5a-Ror signaling is highly conserved and critical to tissue morphogenesis in a variety of vertebrates. However, despite the significance of Wnt5a-Ror signaling in both normal development and disease contexts, the mechanisms by which Wnt5a signals are transmitted and processed within the cell remain unclear. Progress within the field is further hampered by a lack of consensus regarding the number of non-canonical pathways, the biochemical nature of their regulation, and variability in the methods used to measure signaling (Veeman et al., 2003).

To deepen our understanding of Wnt5a-Ror signaling, we have taken systematic approaches to identify specific downstream cellular events that occur in response to pathway activation. In a previous study, we genetically ablated Ror1 and Ror2 receptors in primary mouse embryonic fibroblast (MEF) cultures and used a

proteomic approach to identify downstream signaling events that are misregulated in these cells. From this analysis, we identified the atypical kinesin Kif26b as a downstream component of Wnt5a-Ror signaling that is targeted for degradation upon pathway activation (Susman et al., 2017). We hypothesized that additional downstream regulatory targets likely exist, and the identification of such factors would augment our mechanistic understanding of Wnt5a-Ror signaling. In this study, we conducted a second large-scale proteomic screen to identify additional cellular proteins whose abundance and phosphorylation state are altered by acute stimulation of Wnt5a-Ror signaling. This screen identified the E3 ubiquitin ligase Pdzrn3 as a novel regulatory target of Wnt5a-Ror signaling. Notably, previous studies have identified a binding interaction between Pdzrn3 and Dvl3, as well as role for Pdzrn3 in a variety of morphogenetic cell behaviors, including synaptic growth and maturation, vascular morphogenesis, and neuronal positioning (Lu et al., 2007, Sewduth et al., 2014, Baizabal et al., 2018). Mechanistically, we discovered that Pdzrn3 is degraded in response to Wnt5a-Ror signaling by a mechanism that is independent of β -catenin but dependent on the ubiquitin-proteasome system (UPS). This regulation is mediated by a signaling cascade involving Frizzled (Fzd), Dishevelled (Dvl), Casein kinase 1 (CK1), and Glycogen synthase kinase 3 (GSK3) that is epistatically distinct from Kif26b. Further, we determined that upon Wnt5a stimulation, Pdzrn3 is phosphorylated at three specific amino acid residues on its C-terminal LNX3H domain, and that the phosphorylation of these sites is required for Pdzrn3 degradation. Lastly, we demonstrated that the conserved LNX3H domain is required for Wnt5a-dependent degradation of not only Pdzrn3 but also its structural homolog Lnx4. This suggests that the LNX3H domain may generally function as a Wnt5a-responsive domain. Together, these findings support a role for Pdzrn3 in Wnt5a-Ror signal transduction and provide a platform from which a deeper mechanistic understanding of non-canonical Wnt signaling can be attained.

Results

Large-scale proteomic screen identifies the E3 ubiquitin ligase Pdzrn3 as a downstream regulatory target of Wnt5a-Ror signaling

To profile both early and late molecular events driven by Wnt5a-Ror signaling, we conducted a large-scale proteomic screen in which we acutely stimulated E12.5 primary *Wnt5a* KO MEFs (Ho et al., 2012, Susman et al., 2017, Yamaguchi et al., 1999) with purified recombinant Wnt5a (rWnt5a) for 0, 1 or 6 hours,

and then used quantitative tandem mass tag (TMT) mass spectrometry to globally assess changes in the abundance and phosphorylation state of cellular proteins over time (Figure 1A) (Ting et al., 2011). For rigor and reproducibility, two independent replicates of *Wnt5a* KO MEF cultures were stimulated with rWnt5a and analyzed.

In both analyses of protein level and phosphorylation changes, we defined potential proteins of interest as those with tryptic peptides or phospho-tryptic peptides that exhibited (1) a negative or positive change of > 1.5-fold in abundance and (2) a change with a p-value < 0.05 across the two experimental replicates. Based on these criteria, our top candidate was *Pdzn3*, an E3 ubiquitin ligase, which exhibited significant changes in both steady-state protein abundance and phosphorylation state after rWnt5a stimulation. Although 1 hour of rWnt5a stimulation did not result in detectable changes in *Pdzn3* abundance (Figure 1B), after 6 hours of rWnt5a stimulation we observed that *Pdzn3* abundance was significantly downregulated by 1.72-fold ($p=0.013$, Figure 1C and 1F; Table 1). Additionally, we identified multiple phospho-tryptic peptides derived from two different regions of *Pdzn3* that exhibited significant changes after rWnt5a stimulation (Figure 1D and 1E). A phospho-tryptic peptide containing S843 and S845 (Figure 1G) and another one containing T955, T956 and S962 (Figure 1I) both showed an initial increase at 1 hour, followed by a decrease at 6 hours. Likewise, a third phospho-tryptic peptide containing S775 (Figure 1J), though not scored initially based on its significance value ($p=0.076$), also exhibited a similar pattern of change. Lastly, a phospho-tryptic peptide containing S845 (Figure 1H) decreased gradually after 1 hour and more extensively after 6 hours. Importantly, all phospho-tryptic peptides decrease by 6 hours (Figure 1G-1J) to a similar extent as that of the non-phosphorylated tryptic peptide (Figure 1F). This overall pattern thus raised the hypothesis that Wnt5a signaling first induces the phosphorylation of *Pdzn3* at specific sites at 1 hour, followed by downregulation of *Pdzn3* protein abundance at 6 hours, and these two biochemical events are kinetically and mechanistically coupled.

In addition to *Pdzn3*, the proteomic screen also identified several other known components of the Wnt5a-Ror signaling pathway (Table 1). At both the 1 hour and 6 hour timepoints, a phospho-tryptic peptide from *Kif26b* was scored as a “hit” (1.70- and 2.03-fold decrease, respectively). At the 6 hour timepoint, a phospho-tryptic peptide from CK1 isoform gamma-3 was also scored as a “hit” (1.52-fold increase). In addition, a phospho-tryptic peptide from *Dvl2* exhibited a 1.49-fold increase in abundance after 6 hours of rWnt5a

stimulation. The identification of these previously described Wnt5a signaling targets further validates the selectivity and sensitivity of the proteomic screening approach.

To independently confirm that *Pdzn3* abundance is indeed regulated by Wnt5a signals, we generated rabbit polyclonal antibodies against *Pdzn3* and used western blotting to analyze the steady-state cellular levels of *Pdzn3* after rWnt5a stimulation. Consistent with our proteomic screening results, we observed that the abundance of *Pdzn3* significantly decreases after 6 hours of rWnt5a stimulation (Figure 2A and 2B). This change parallels other previously described responses of Wnt5a-Ror signaling, including an increase in the phosphorylation of Ror1, Ror2 and Dvl2, and a decrease in Kif26b abundance (Figure 2A and 2B) (Ho et al., 2012, Susman et al., 2017).

To test whether Ror receptors are required for Wnt5a signaling to *Pdzn3*, we took advantage of conditional Ror receptor family knockout MEFs derived from E12.5 *Ror1^{fl/fl}; Ror2^{fl/fl}; CAG-CreER* embryos. These MEFs undergo robust autocrine/paracrine Wnt5a-Ror signaling even in the absence of exogenously added Wnt5a (Ho et al., 2012). To genetically ablate *Ror1* and *Ror2* expression in these MEFs, we treated the cells with 4-hydroxytamoxifen (4OHT) to induce CreER-mediated deletion of the *Ror1^{fl/fl}* and *Ror2^{fl/fl}* alleles. We observed that loss of Ror receptor expression resulted in a significant increase in *Pdzn3* levels which correlated with a decrease in Dvl2 phosphorylation as well as an increase in Kif26b abundance (Figure 2C and 2D). These results indicate that regulation of *Pdzn3* abundance by endogenous Wnt5a requires Ror receptors.

In addition to post-transcriptional regulation of *Pdzn3*, we questioned whether Wnt5a might regulate *Pdzn3* transcriptionally as well. To test this hypothesis, we treated *Wnt5a* knockout MEFs with rWnt5a for 1 or 6 hours and analyzed the levels of *Pdzn3* mRNA by reverse transcription-quantitative polymerase chain reaction (RT-qPCR). Unlike *Pdzn3* protein, *Pdzn3* transcripts do not change significantly after 1 or 6 hours of rWnt5a stimulation (Figure 2E), indicating that Wnt5a-Ror signaling regulates *Pdzn3* protein abundance through a post-transcriptional mechanism. Overall, these experiments establish that regulation of *Pdzn3* protein abundance is a major response of Wnt5a-Ror signaling.

A non-canonical Wnt signaling cascade involving Fzd, Dvl, CK1, GSK3 and the ubiquitin-proteasome system regulates *Pdzn3* degradation

To dissect the molecular mechanisms that mediate Wnt5a regulation of Pdzrn3, we designed a flow cytometry-based reporter in which we stably expressed GFP-Pdzrn3 in NIH/3T3 cells (or WRP reporter cells for Wnt5a-Ror-Pdzrn3, Figure 3A). Consistent with our observations in primary *Wnt5a* knockout MEFs, treatment of the WRP reporter cells with rWnt5a for 6 hours resulted in a significant downregulation of GFP-Pdzrn3 reporter signal, thereby demonstrating the fidelity of this reporter assay. Moreover, we established that a saturable dose-dependent relationship exists between rWnt5a concentrations and GFP-Pdzrn3 downregulation, with a calculated EC₅₀ of 77.1 ng/mL, which is similar to other Wnt induced responses (Figure 3B) (Bryja et al., 2007b, Witze et al., 2008, Ho et al., 2012, Connacher et al., 2017, Witze et al., 2013, Park et al., 2015). This supports the physiological relevance of Pdzrn3 downregulation.

We next used the WRP reporter cells to investigate the biochemical nature of Pdzrn3 downregulation. We pharmacologically tested the role of the ubiquitin-proteasome system (UPS) in Pdzrn3 downregulation as UPS is a major regulatory pathway involved in many signaling systems, and our previous study demonstrated that it is required for Wnt5a-dependent degradation of Kif26b (Susman et al., 2017). We treated WRP cells with a panel of small-molecule inhibitors that block different components of the UPS: epoxomicin, which targets the proteasome (Meng et al., 1999); PYR-41, which targets the ubiquitin E1 ubiquitin ligase (Yang et al., 2007); and MLN4924, which targets Cullin E3 ligases (Tong et al., 2017). Each of these drugs significantly inhibited Wnt5a-dependent Pdzrn3 downregulation (Figure 3C), indicating that the UPS and the Cullin family of E3 ligases are required for Wnt5a-dependent degradation of Pdzrn3.

To test whether Wnt5a-Ror-dependent Pdzrn3 degradation occurs via a non-canonical Wnt signaling mechanism independent of the Wnt/ β -catenin pathway, we treated WRP reporter cells with Dkk-1 and IWR-1-endo, which block canonical Wnt/ β -catenin signaling at the receptor and destruction complex level, respectively (Bafico et al., 2001, Lee et al., 2003, Huang et al., 2009). We observed that neither inhibitor blocked Wnt5a-induced degradation of GFP-Pdzrn3, indicating that this regulation occurs independently of the canonical Wnt pathway (Figure 3D). However, we also noted that both inhibitors, in the absence of Wnt5a treatment, slightly increased the basal fluorescence of the GFP-Pdzrn3 reporter; the mechanism behind this regulation is currently unclear. Nevertheless, our data demonstrate that Wnt5a-Ror-Pdzrn3 signaling is a bona fide non-canonical Wnt pathway.

We next investigated if other established Wnt signaling mediators are also involved in Pdzrn3 degradation. We focused our analysis on the Fzd1, Fzd2, and Fzd7 subfamily of Fzd receptors and all three members of the family of Dvl scaffolding proteins based on their emerging connection to Robinow syndrome (Afzal et al., 2000, Afzal and Jeffery, 2003, Person et al., 2010, Bunn et al., 2015, White et al., 2015, White et al., 2016, White et al., 2018). We overexpressed mouse Fzd1, Fzd2, or Fzd7 and human DVL1, DVL2 or DVL3 in WRP reporter cells via lentivirus-mediated transduction and observed that overexpression of each Fzd and DVL protein mimicked the effect of Wnt5a by decreasing the WRP reporter signal significantly, whereas overexpression of the myc epitope as a negative control did not decrease WRP reporter fluorescence. These findings suggest that Fzd and DVL family proteins function epistatically downstream of Wnt5a to regulate Pdzrn3 degradation (Figure 3E and 3F).

In addition to Fzd receptors and DVL scaffolding proteins, several kinases are known to be involved in Wnt signaling; specifically, GSK3 and CK1 have been reported to phosphorylate Ror receptors (Yamamoto et al., 2007; Grumolato et al., 2010), and Dvl2 and Dvl3 (Bryja et al., 2007a, Bryja et al., 2007b), respectively. Whether these phosphorylation events are required for Wnt5a-dependent regulation of Pdzrn3, however, remains unknown. To examine this hypothesis, we treated WRP reporter cells with small-molecule inhibitors targeting CK1 (D4476) or GSK3 (CHIR99021). We noticed that both treatments significantly reduce Wnt5a-induced GFP-Pdzrn3 degradation (Figure 3G), thus demonstrating that both CK1 and GSK3 play a functional role in Wnt5a-Ror-Pdzrn3 signal transduction.

We previously reported that the atypical kinesin Kif26b is another downstream regulatory target of Wnt5a-Ror signaling (Susman et al., 2017, Karuna et al., 2018). Because Pdzrn3 and Kif26b are both regulated by the Wnt5a-Ror-Dvl axis, we sought to define the epistatic relationship between Pdzrn3 and Kif26b (i.e., whether these two proteins functions in a linear cascade or in parallel branches). To distinguish these possibilities, we used CRISPR/Cas9 gene editing to generate cells lacking Kif26b and its homolog Kif26a (Supplemental Figure 3), which we previously showed is also a target of Wnt5a-Ror signaling (Karuna et al., 2018), and tested whether GFP-Pdzrn3 is still degraded upon rWnt5a stimulation. Our result demonstrated that genetic deletion of *Kif26a* and *Kif26b* does not hinder the ability of rWnt5a to induce Pdzrn3 degradation (Figure 3H). In the converse experiment, we generated cells lacking Pdzrn3 and its homolog Lnx4, which possesses a structure highly similar to Pdzrn3 (see Figure 4E), and observed that rWnt5a-induced GFP-Kif26b

degradation still occurred (Figure 3I), indicating that, like *Pdzn3*, the ability of *Wnt5a* to signal to *Kif26b* is not lost with genetic removal of *Pdzn3* and *Lnk4*. While we suspect the slight, but statistically significant, variations in *Pdzn3* and *Kif26b* degradation may be due to the clonal nature of the *Kif26a/Kif26b* double KO and *Pdzn3/Lnk4* double KO cells, respectively, our experiment does not formally rule out the possibility that there are some functional interactions between *Kif26b* and *Pdzn3*. Nonetheless, our findings are most consistent with the notion that *Kif26b* and *Pdzn3* are regulated and degraded independently of each other by *Wnt5a*-*Ror* signaling downstream of *Dvl*.

Degradation of *Pdzn3* and its related homologs requires *Wnt5a*-dependent phosphorylation of their C-terminal LNX3H domains

We next sought to define the domain(s) of *Pdzn3* required for its degradation and explore the possible role of phosphorylation in this regulation. *Pdzn3* is a cytosolic protein that contains an N-terminal RING domain that confers its putative E3 ligase activity, two internal PDZ domains that mediate protein-protein interactions, a C-terminal LNX3 homology (LNX3H) domain with no known function, and a C-terminus PDZ domain binding motif (Figure 4A) (Flynn et al., 2011, Sewduth et al., 2014). The six phospho-tryptic peptides discovered in our phosphoproteomic analysis cluster into two groups: Group 1 phosphorylation sites (S775, S843, and S845) reside within the linker region between the second PDZ domain and the C-terminal LNX3 homology (LNX3H) domain, and Group 2 phosphorylation sites (T955, T956, and S962) are located within the LNX3H domain itself. Interestingly, while phosphorylation of Group 1 sites showed only a slight increase at 1 hour and then decreased after 6 hours (compare Figure 1F with 1G, 1H, 1J), phosphorylation of Group 2 sites increased drastically after 1 hour of *rWnt5a* stimulation, prior to *Pdzn3* degradation, and then decreased after 6 hours of *rWnt5a* stimulation (compare Figure 1F with 1I), raising the hypothesis that phosphorylation of these sites, particularly those in Group 2, may be required for *Wnt5a*-regulation of *Pdzn3* degradation.

To test this hypothesis, we systematically generated phosphoinhibitory mutants (T or S to A substitutions) of all three sites in either Group 1 or Group 2 and examined the effects of these mutations on *rWnt5a*-induced *Pdzn3* degradation. We observed that while mutation of Group 1 sites had no effect on *rWnt5a*-induced *Pdzn3* degradation, mutation of Group 2 sites strongly abolished GFP-*Pdzn3* degradation (Figure 4B). To further dissect which specific sites within Group 2 are required for *Pdzn3* degradation, we

individually mutated each of the three sites and discovered that any of the three single mutations significantly reduced rWnt5a-induced GFP-Pdzrn3 degradation (Figure 4C). To further test whether phosphorylation of these three residues is sufficient to induce Pdzrn3 degradation, we generated a triple phosphomimetic mutant (T or S to E) and observed that these mutations, in the absence of exogenous rWnt5a stimulation, constitutively decreased the Pdzrn3 reporter signal to a level comparable to that of wild-type Pdzrn3 upon rWnt5a stimulation, and no further degradation was observed upon rWnt5 stimulation (Figure 4D). These experiments establish that Wnt5a-dependent phosphorylation of the three Group 2 sites in the LNX3H domain is both required and sufficient to drive Pdzrn3 degradation.

Pdzrn3 has several homologs that together make up the Ligand of Numb-X or Lnx family of E3 ligases (Figure 4E). Like Pdzrn3, each Lnx family member possesses an N-terminal RING domain (with the exception of Lnx5) and one to four internal PDZ binding domains; additionally, Lnx4 and Lnx5 each possess a C-terminal LNX3H domain and a C-terminus PDZ domain binding motif (Flynn et al., 2011, Sewduth et al., 2014). Notably, the Group 2 phosphorylation sites located within the LNX3H domain are conserved in Lnx4 and Lnx5 (Figure 4F). Based on our data indicating that these sites regulate Wnt5a-induced Pdzrn3 degradation, we hypothesized that Lnx4 and Lnx5 may also be regulated by Wnt5a signals and that the LNX3H domain may generally function as a Wnt5a-responsive domain. To test this hypothesis, we generated reporter cell lines stably expressing GFP-Lnx1, -Lnx2, -Lnx4, or -Lnx5 fusion proteins and assessed their ability to undergo degradation in response to rWnt5a stimulation. As predicted, when stimulated with rWnt5a, GFP-Lnx1 and GFP-Lnx2, which lack an LNX3H domain, did not degrade, whereas GFP-Lnx4, which has an LNX3H domain, exhibited a modest but significant decrease (Figure 4G). Interestingly, GFP-Lnx5, which also has an LNX3H domain but lacks a RING domain, was not degraded in response to rWnt5a stimulation (Figure 4G). We therefore conclude that like Pdzrn3, Lnx4 is also a target of Wnt5a signaling. Further, the Wnt5a responsiveness of Lnx family members correlates with the presence of both LNX3H and RING domains, as the primary difference between Lnx5 and Pdzrn3/Lnx4 is the N-terminal RING domain.

To further test the idea that the LNX3H domain might act as a Wnt5a-responsive domain, we generated truncation mutants of GFP-Pdzrn3 and GFP-Lnx4 lacking this domain. When we expressed the mutant Pdzrn3 and Lnx4 reporters in NIH/3T3 cells, not only was Wnt5a-induced degradation completely abolished (Figure 4H and 4I), but the steady-state fluorescence of unstimulated reporter cells was also substantially reduced (Figure

4H and 4I). These observations suggest that the LNX3H domain of Pdzrn3 and Lnx4 acts not only as a Wnt5a-responsive domain but may do so by regulating overall protein stability, possibly through functional modulation of the N-terminal RING domain. While the precise mechanism by which the LNX3H domain integrates Wnt5a signals remains unknown and is beyond the scope of this study, our finding defines the LNX3H domain as a bona fide Wnt5a-responsive domain that regulates Pdzrn3 and LNX4 stability.

Discussion

In this study, we conducted a whole proteome-scale mass spectrometry screen in primary *Wnt5a* knockout MEFs to identify early and late downstream events driven by Wnt5a-Ror signaling and identified the E3 ubiquitin ligase Pdzrn3 as a novel target. Activation of Wnt5a-Ror signaling results in the regulation of Pdzrn3 abundance in a β -catenin independent manner mediated by a signaling cascade involving Fzd receptors, Dvl scaffolding proteins, GSK3, and CK1 that culminates in UPS-dependent degradation of Pdzrn3; this regulation is epistatically distinct from Kif26b degradation, another target of Wnt5a-Ror signaling that we previously reported (Figure 4J). For degradation to occur, Pdzrn3 requires Wnt5a-dependent phosphorylation of three specific amino acid residues in its C-terminal LNX3H domain, which is highly conserved across other homologs of Pdzrn3 and in other organisms. Mutation of these residues alone or together blocks Wnt5a-induced Pdzrn3 degradation, whereas truncation of the LNX3H domain results in constitutive destabilization of Pdzrn3 even in the absence of Wnt5a, suggesting that the LNX3H domain may function as both a Wnt5a-responsive domain and an intrinsic regulator of Pdzrn3 stability. Based on these findings, we propose that the LNX3H domain of Pdzrn3 may function to prevent Pdzrn3 auto-ubiquitination and self-degradation mediated by its RING domain. Prior to Wnt5a stimulation, Pdzrn3 may adopt a “closed” conformation as its C-terminal PDZ domain binding motif interacts with one of its internal PDZ domains to block its E3 ligase activity. Upon Wnt5a stimulation, Pdzrn3 is C-terminally phosphorylated on its LNX3H domain by a yet unidentified kinase to switch the “closed” conformation into an “open” conformation, allowing Pdzrn3 to catalyze the ubiquitination of relevant substrates as well as itself. Notably, this “opened/closed” conformation paradigm has been previously described in other components of Wnt signaling, including Axin and Dvl (Kim et al., 2013, Lee et al., 2015, Qi et al., 2017). Conceivably, the equilibrium between the “closed” and “open” Pdzrn3 could be modulated through either intramolecular interactions within a single Pdzrn3 molecule or through intermolecular interactions between

Pdzrn3 dimers or multimers. Future detailed biochemical experiments are required to directly dissect these possibilities.

It is well established that several components of canonical Wnt signaling (e.g., β -catenin, adenomatous polyposis coli (APC), and Axin) are regulated by proteasomal degradation (Papkoff et al., 1996, Choi et al., 2004, Huang et al., 2009). The present work, together with other recent studies, establishes that several effectors of non-canonical Wnt pathways, including Pdzrn3, Kif26a, Kif26b and Syndecan 4, are also subject to regulation by the ubiquitin-proteasome pathway (Carvallo et al., 2010, Susman et al., 2017, Karuna et al., 2018). Collectively, these findings suggest that regulated proteolysis to tune the abundance of downstream effectors and thus, signaling outcomes, may be a paradigm common to both canonical and non-canonical Wnt signaling pathways. This concept will continue to evolve as additional Wnt signaling components are discovered and characterized.

Although our study focuses on the biochemical regulation of Pdzrn3 by Wnt5a-Ror signaling, previous work by others supports the physiological importance of Pdzrn3 in non-canonical Wnt signaling. One particularly notable study focuses on the role of Pdzrn3 in developmental vascular morphogenesis (Sewduth et al., 2014). In this study, Sewduth et al. identified a binding interaction between Pdzrn3 and Dvl3 via a yeast 2-hybrid screen and subsequent co-immunoprecipitation, going on to demonstrate that loss of Pdzrn3 *in vivo* results in increased vasculature disorganization in both embryonic yolk sacks and the developing mouse brain. Furthermore, deletion of Pdzrn3 *in vitro* led to decreased persistent directional migration in human umbilical vein endothelial cells. Collectively, these findings indicate that loss of Pdzrn3 results in non-canonical Wnt signaling defects that can be observed at the molecular, cell behavioral, and organismal levels, which, along with our study, suggests a highly physiologically relevant role for Pdzrn3 in Wnt5a-dependent morphogenetic regulation.

Interestingly, our genetic epistasis experiments suggest that Wnt5a-Ror signaling regulates Pdzrn3 and Kif26b independently of each other. Based on these observations, how might Kif26b and Pdzrn3 work together to ultimately regulate cell processes? We envision that these effectors may have evolved distinct functions that work in concert to orchestrate cell and tissue morphogenetic behavior. While Pdzrn3 has been shown to be involved in cell migration as described earlier, Kif26b has been linked to the regulation of cell adhesion (Uchiyama et al., 2010). In future studies, *in vivo* mouse genetics in conjunction with cell biological analyses

should help elucidate whether Wnt5a-Ror signaling concomitantly regulates these complementary cell adhesion and cell migration functions to coordinately drive various morphogenetic events.

The historical lack of quantitative and reliable readouts for Wnt5a-Ror signaling has been a major limitation in the field. We leveraged our discovery of Pdzn3 and its regulation by Wnt5a-Ror signaling to develop a new flow cytometry-based reporter that enables sensitive and quantitative detection of pathway activity in live cells. In addition to dissecting the mechanisms that mediate Pdzn3 degradation, this reporter assay could also be utilized to interrogate any biochemical steps in the pathway upstream of Pdzn3, understand various disease-associated mutations, and serve as an important platform for high throughput screening of small molecules that target Wnt5a-Ror-driven developmental disorders and cancers.

Materials and methods

Cell lines

Primary MEFs were isolated directly from mouse embryos as described (Ho et al., 2012) and used within 3 passages. NIH/3T3 Flp-In (R76107, Thermo Fisher Scientific) cells were purchased and were not re-authenticated; cells tested negative for mycoplasma contamination using the Universal Mycoplasma Detection Kit (30-1012K, ATCC). All cell lines were cultured at 37 degree C and 5% CO₂ in Dulbecco's Modified Eagles Medium (MT15017CV, Corning) supplemented with 1x glutamine (25-005-CI, Corning), 1x penicillin-streptomycin (30-002-CI, Corning) and 10% fetal bovine serum (16000069, Thermo Fisher Scientific).

TMT/MS3 proteomic screen

Primary *Wnt5a*^{-/-} MEFs (derived and pooled from three different E12.5 *Wnt5a*^{-/-} embryos) were seeded in 6 10-cm plates at 50% confluency 3 days before rWnt5a stimulation (day 0), such that cells would have become fully confluent for 2 days. On the day of stimulation (day 3), cells in each 10-cm plate were treated either with rWnt5a (100ng/mL final concentration) for 1h or 6hr, or with the control buffer (1x PBS, 0.1% bovine serum albumin, 0.5% w/v CHAPS) for 6hr. The entire stimulation experiment was conducted in two independent replicates. At the end of the Wnt5a stimulation time course, cells were washed once with ice-cold PBS and plates were scraped into 1 mL of ice-cold lysis buffer (8 M urea, 75 mM NaCl, 50 mM Tris pH 8.2, 1 mM NaF, 1 mM β-glycerophosphate, 1 mM Na₃VO₄, 10 mM Na₄P₂O₇, 1 mM PMSF, and Complete protease inhibitor (-

EDTA, Roche)). Cells were homogenized by pipetting up and down using a P-1000 and then sonicated in a Bioruptor (17 x 30s ON/OFF cycles). Cell lysates were then centrifuged at 40,000 RPM for 20 min at 4C. The clarified high-speed supernatants were collected, snap frozen in liquid nitrogen and stored at -80C until the TMT/MS3 analysis was performed. Protein concentrations were determined using BCA reagents (Pierce) and normalized.

To perform the TMT/MS3 screen, tryptic peptides were prepared from whole cell lysates and the peptide mixtures from the different experimental conditions were labeled with the six TMT reagents, such that reporter ions at m/z of 126, 127, 128, 129, 130 and 131 would be generated in the tandem spectrometry. Phosphopeptides were enriched by TiO₂ chromatography. Liquid chromatography, MS3 tandem mass spectrometry and data analysis were carried out as previously described (Ting et al., 2011, McAlister et al., 2014, Paulo et al., 2015).

Cloning of mouse *Pdzrn3*, *Lnx1*, *Lnx2*, *Lnx4*, and *Lnx5* cDNA

For cloning of mouse *Pdzrn3* cDNA, a first strand cDNA pool was generated from MEF total RNA Maxima H Minus reverse transcriptase and oligo dT primers according to manufacturer's instructions (EP0751, ThermoFisher Scientific). This cDNA library was then used as template for PCR amplification of the *Pdzrn3* open reading frame with the following primers, Forward: gatcGGCCGGCCtACcAtgggttctgagttgatcgc; Reverse: gatcGGCGCGCCTTATACAGTAGTCACCGACAGGAA. The PCR product was subcloned into a modified pCS2+ vector using the FseI and AsclI restriction sites. The entire *Pdzrn3* open reading frame was confirmed by Sanger sequencing.

For cloning the *Lnx1*, *Lnx2*, *Lnx4*, and *Lnx5* cDNAs, the same workflow was used, except that E14.5 mouse brain RNA was used to generate the first strand cDNA pool, and the following primers were used to PCR amplify and subclone the respective cDNAs: mLnx1 forward, gatcGGCCGGccTACcAtgaaccaaccggaccttgcatg; mLnx1 Reverse, gatcGGCGCGCCTTATAAAAAAGTACCAGGCCAAGAAG; mLnx2 forward, gatcGGCCGGccTACcAtgggaacaaccagtgcgagatgg; mLnx2 reverse, gatcGGCGCGCCCTATACGAGGCTGCCTGGCCAGCAG; mLnx4 forward,

gatcgccggccTaccATGGGCTTCGCTTTGGAGCGTCTC; mLnx4 reverse,
gatcGGCGCGCCtcaTACGGTGGTCACCGACAGAAAGGC; mLnx5 forward,
gatcGGCCGgCCTACCatgggatgtaatatgtgtgtggtc; mLnx5 reverse,
gatcGGCGCGCCTCAGACAGTGGTGACAGAGAGCAG. All constructs were confirmed by Sanger sequencing.

Antibodies

Antibodies against Ror1, Ror2, and Kif26b were described previously (Ho et al., 2012, Susman et al., 2017). The following antibodies were purchased: rabbit anti-Dvl2 (#3216, Cell Signaling) and mouse anti- α -tubulin (clone DM1A, #ab7291, Abcam).

Initial analyses of Pdzn3 were conducted using a commercial antibody (SC-99507, Santa Cruz Biotechnology); however, the antibody was discontinued and all subsequent analyses (including all data presented in this paper) were conducted using anti-Pdzn3 antibodies produced in-house. To generate anti-Pdzn3 antisera, rabbits were immunizing with a mixture of two different antigens: 1) a synthetic peptide with the sequence LLTHGTKSPDGTRVYNSFLSVTC, conjugated to keyhole limpet hemocyanin (77600, ThermoFisher Scientific), and 2) a maltose binding protein N-terminally fused to a Pdzn3 protein fragment extending from amino acids 902 to 1063, recombinantly expressed in and purified from *E. coli*. Antibodies were affinity purified from antisera over a column with a full-length recombinant Pdzn3 protein covalently immobilized to Sepharose beads (AminoLink Plus, 20501, ThermoFisher Scientific). Full length Pdzn3 was expressed in insect cells using the Bac-to-Bac baculovirus expression system (10359016, ThermoFisher Scientific); the protein was insoluble and was purified under denatured conditions using 5.5M guanidinium hydrochloride, coupled to AminoLink Plus Resin, and renatured by gradually removing guanidinium hydrochloride.

Western blotting

Protein lysates for SDS-PAGE and western blotting were prepared in 1x - 2x Laemmli sample buffer or LDS sample buffer (Life Technologies). Protein lysates used for Kif26b western blotting were not heated, as the

Kif26b signal weakens substantially after heating, likely due to heat-induced protein aggregation (Susman et al., 2017). All other protein lysates were heated at 90C for 5 min before SDS-PAGE and western blotting.

Quantitative western blotting was performed using the Odyssey infrared imaging system (Li-Cor Biosciences) according to the manufacturer's instructions. The median background method was used with a border width of two pixels on a sides around the perimeter of the area being quantified. Non-saturated protein bands were quantified by using Odyssey software with the gamma level set at 1.

Generation of stable NIH/3T3 cell lines

To construct the GFP-Pdzrn3 expression plasmid, the eGFP open reading frame was first subcloned into pENTR-2B (Life Technologies), and the full-length mouse Pdzrn3 open reading frame was subcloned in frame to the C-terminus of GFP. The resulting construct was verified by sequencing and then recombined with the pEF5-FRT-V5 vector (Life Technologies) using LR clonase (Life Technologies) to create pEF5-GFP-Pdzrn3-FRT. The pEF5-GFP-Pdzrn3-FRT plasmid was used to generate stable isogenic cell lines using the Flp-In system and Flp-In NIH/3T3 cell line (Life Technologies). DNA transfection was performed in 10-cm plates with Genjet In Vitro Transfection Reagent (SL100488; SignaGen Laboratories). Cells that stably integrate the Flp-In constructs were selected using 200µg/ml hygromycin B and expanded. Cell lines expressing phosphoinhibitory or phosphomimetic Pdzrn3, Lnx1, Lnx2, Lnx4, Lnx5, Pdzrn3ΔLnx3H, and Lnx4ΔLnx3H were similarly created by cloning the open reading frame to the C-terminus of GFP in frame and conducting the workflow described above.

Lentivirus-mediated protein overexpression

Recombinant lentiviruses were generated using the pLEX_307 (for all Fzd and DVL constructs) vectors, which uses the EF1 promoter to drive transgene expression. pLEX_307 was a gift from David Root (Addgene plasmid # 41392). The human DVL1 and DVL3 open reading frames were cloned by PCR from a HeLa cell cDNA pool using the following primers; hDVL1 forward, gatcGAATTCCACCatgggcgagaccaagattatctac; hDVL1 reverse, gatcGGCGCGCCTCACATGATGTCCACGAAGAACTC; hDVL3 forward, TTCAGGCCGGCCTACCATGGGCGAGACCAAGATCATCTAC; hDVL3 reverse,

GAGGCGCGCCTCACATCACATCCACAAAGAAGCTC. Similarly, the human DVL2 open reading frame was cloned by PCR from a separate HeLa cDNA pool. The following primers were used: hDvl2 forward, gctggcgggcgGcCgGccaatggcgggtagcagcactggggg; hDVL2 reverse, gtcgacgGgCGcgcctacataacatccacaaagaactcg. The mouse Fzd1 and Fzd7 open reading frames were PCR amplified from Addgene plasmids #42253 and 42259 (gifts from Jeremy Nathans), respectively, using the following primers: mFzd1 forward, gatcggccggcctaccatggctgaggaggcggcgcttag; mFzd1 reverse, gatcggcgcgccTCAGACGGTAGTCTCCCCCTGTTTG; mFzd7 forward, gatcggccggcctaccatgccccggcggcggcg; mFzd7 reverse, gatcggcgcgccTCATACCGCAGTTTCCCCCTTGC. The mFzd2 open reading frame was cloned via PCR from mouse brain via the following primers: mFzd2 forward, gatcggccggcctaccatgccccggcggcggccttag; mFzd2 reverse, gatcggcgcgccTCACACAGTGGTCTCGCCATGC. The open reading frames of all lentiviral constructs were verified by sequencing. Lentiviruses were packaged and produced in HEK293T cells by co-transfection of the lentiviral vectors with the following packaging plasmids: pRSV-REV, pMD-2-G and pMD-Lg1-pRRE (gifts from Thomas Vierbuchen). 0.75ml or 0.25 ml of the viral supernatants was used to infect GFP-Pdzrn3 reporter cells seeded at 20% confluency in 24-well plates. Puromycin selection (0.002 mg/ml) was carried out for three days. Cells from the viral titer that killed a large proportion of cells (60-90%) were expanded and used for flow cytometry; this ensured that the multiplicity of infection (MOI) is ~1 for all cell lines used in the experiments.

Generation of double knockout cell lines

Kif26b knockout cells were previously described (the mutant clone with +1 and -13 frameshifts, generated using sgRNA 1; (Susman et al., 2017)). This *Kif26b* mutant clone was subject to a second round of mutagenesis to knock out *Kif26a* via CRISPR/Cas9-mediated genome editing according to (Ran et al., 2013). Briefly, a modified version of LentiCRISPR V2 (Addgene #52961), in which the puromycin selection cassette was modified with a blasticidin selection cassette, was used to generate lentiviruses expressing small guide RNAs (sgRNAs) with the following sequence: GCTCGTGGAGCTAAAACGAC. In wild-type NIH/3T3 cells, Pdzrn3 was similarly targeted using the following sequence: AGCTGCCCCGCGCGTTGTTCG. Following lentivirus infection, cells were passaged for 5 days to allow time for mutagenesis to occur. Cells were

subsequently selected using blasticidin (0.002mg/mL) in the case of *Kif26a* mutagenesis, or puromycin (0.002mg/mL) in the case of *Pdzrn3* mutagenesis. Individual cell clones were picked from cell populations targeted with each of these sgRNAs, expanded and then validated by deep sequencing the relevant genomic regions amplified by PCR.

To generate *Pdzrn3/Lnx4* double knockout cells, *Pdzrn3* knockout NIH/3T3 cells were electroporated with CRISPR/Cas9 ribonucleoprotein complexes targeting *Lnx4* using the following gRNA sequence: GCCAACAUCCGGCAUGACUCGUUUUAGAGCUAUGCU. 24 hours after electroporation, cells were subjected to fluorescence activated cell sorting (MoFlo Astrios Cell Sorter, Beckman Coulter, 561nm laser) to plate individual cells in 96-well plates; cells were allowed to recover for two weeks prior to expansion and validation of mutations via deep sequencing the relevant genomic regions amplified by PCR.

Recombinant proteins and inhibitors

The following recombinant proteins and drugs were purchased: human/mouse *Wnt5a* (654-WN-010, R&D Systems); *Wnt-C59* (C7641-2s; Cellagen Technology); epoxomicin (A2606, ApexBio); PYR-41 (B1492, ApexBio); MLN4924 (I50201M, R&D systems); mouse *Dkk-1* (5897-DK-010, R&D Systems); IWR-1-endo (B2306, ApexBio); D4476 (A3342, ApexBio); and CHIR99021 (A3011, ApexBio).

Reverse transcription and qPCR

Total RNA was isolated from *Wnt5a* KO MEFs stimulated with r*Wnt5a* for 0, 1, or 6 hours using the RNeasy Plus Mini Kit (Qiagen, #74134), and cDNA was synthesized using QuantiNova Reverse Transcription Kit (Qiagen, #205411), both according to the manufacturer's instructions. The cDNA was the source of input for qPCR, using QuantiNova SYBR Green PCR Kit (Qiagen, #208054). The following qPCR primer pairs were used: m*Pdzrn3* forward, CTGCGCTACCAGAAGAAGTTC; m*Pdzrn3* reverse, TCCATCTTGATTGTCCACACAG; m*Gapdh* forward, AGGTCGGTGTGAACGGATTTG; m*Gapdh* reverse, TGTAGACCATGTAGTTGAGGTCA.

Flow cytometry

NIH/3T3 cells were plated at a density of 0.09-0.095M/well in 48-well plates either directly in complete media containing Wnt5-C59 (10nM) or in complete media and later changed to complete media containing Wnt-C59 24 hours after plating; all rWnt5a stimulations and inhibitor pretreatments and treatments were conducted in the presence of Wnt-C59. 48 hours after plating, cells were stimulated with rWnt5a for 6 hours. For inhibitor treatments, cells were pretreated with the appropriate inhibitor for 1 hour prior to rWnt5a treatment for 6 hours in the presence of the same inhibitor. Cells were then harvested, resuspended in PBS + 0.5% FBS and analyzed using a flow cytometer (Becton Dickinson FACScan, 488nm laser). Raw data were acquired with CellQuest (Becton Dickinson) and processed in FlowJoX (Treestar, Inc). Processing entailed gating out dead cells, calculation of median fluorescence, percent change of medians, and overlay of histograms. Dose-response curves based on percent change were fitted in Prism (GraphPad Software).

Acknowledgements

We thank the members of the Ho and Jao labs at UC Davis for their input and discussions. We thank Karl Willert for carefully reading of the manuscript. We acknowledge Bridget McLaughlin and Jonathan Van Dyke at the UC Davis Cancer Center Flow Cytometry core for their training and technical assistance (supported by NCI P30 CA093373). We thank Mikaela Louie and Alec Snavely for their assistance with MatLab. We also thank Ryan Toedebusch and Christine Toedebusch for discussions about CRISPR targeting strategies as well as Xueer Jiang, Jose Uribe Salazar, and Megan Dennis for their assistance with CRISPR mutation analysis. This work was supported by National Institutes of Health grant 1R35GM119574 and American Cancer Society grant IRG-95-125-13 to H.H. Ho.

Figure legends

Figure 1. Identification of the E3 ubiquitin ligase Pdzn3 as a downstream regulatory target of Wnt5a-Ror signaling. A) Workflow of whole cell proteomics screen. Primary MEF cultures were generated from *Wnt5a* knockout E12.5 mouse embryos and stimulated with rWnt5a (0.1µg/mL) for 0, 1, or 6 hours. After rWnt5a stimulation, whole cell lysates were collected and processed for LC/MS3 tryptic/phospho-tryptic peptide identification and quantification, as described in the main text and Materials and Methods. The rWnt5a

stimulation and proteomic analysis were conducted in two independent technical replicates. **B and C**) Volcano plots showing changes in the abundance of detected tryptic peptides in response to rWnt5a stimulation (0.1 μ g/mL) after 1 hour (B) or 6 hours (C). The abundance of a tryptic peptide from Pdzn3 (orange dots) changed strongly after 6 hours of rWnt5a stimulation. **D and E**) Volcano plots showing changes in the abundance of detected phospho-tryptic peptides after 1 hour (D) or 6 hours (E) of rWnt5a stimulation (0.1 μ g/mL). A total of five phosphosites from Pdzn3 (S843, S845, T955, T956, and S962), grouped in two clusters based on their location in the protein, were detected and exhibited distinct patterns of changes after rWnt5a stimulation (orange dots). **F through I**) Line plots showing Wnt5a-induced changes in the abundance of individual tryptic (F) or phospho-tryptic peptides (G through I) from Pdzn3 after 1 hour or 6 hours of rWnt5a stimulation. **J**) A sixth phospho-tryptic peptide site (S775) did not pass the initial filter (p-value = 0.076), but also showed clear changes with rWnt5a stimulation. Error bars represent \pm SEM calculated from two technical replicates.

Figure 2. Validation of Pdzn3 as a downstream regulatory target of Wnt5a-Ror signaling. **A)** Western blot showing downregulation of Pdzn3 steady-state levels in response to rWnt5a stimulation. Primary *Wnt5a* knockout MEF cultures (n=3, biological replicates) were stimulated with rWnt5a (0.2 μ g/mL) for 0, 1, or 6 hours, and membranes were blotted with antibodies against Kif26b, Pdzn3, Ror1, Ror2, Dvl2 and Tubulin. The decrease in Pdzn3 abundance correlated with other known indicators of Wnt5a-Ror signaling, including phosphorylation changes in Ror1, Ror2, and Dvl2 and a decrease in Kif26b abundance. Experiments from two representative biological replicates are shown. **B)** Quantification of the western blotting experiments shown in (A). Error bars represent \pm SEM calculated from three biological replicates. t-test (unpaired) was performed to determine statistical significance for the following comparisons: 1hr vs. 0hr; 6hr vs. 0hr. **C)** Western blots showing the requirement of endogenous Ror receptors for Pdzn3 regulation. Primary MEFs derived from *Ror1^{fl/fl}*; *Ror2^{fl/fl}*; *ER-cre* embryos were treated with 4-hydroxytamoxifen (4-OHT) to induce genetic ablation of *Ror1* and *Ror2*. Protein lysates were analyzed by western blotting using antibodies against Kif26b, Pdzn3, Ror1, Ror2, Dvl2 and Tubulin. An increase in Pdzn3 and Kif26b steady-state abundance along with a decrease in Dvl2 phosphorylation correlated with the genetic loss of *Ror1* and *Ror2* expression. **D)**

Quantification of the western blotting experiments shown in (C). Error bars represent \pm SEM calculated from three biological replicates. t-test (unpaired) was performed to determine statistical significance for the following comparisons: +4OHT vs. -4OHT. **E**) Plot showing the effect of Wnt5a stimulation on *Pdzn3* transcript levels. Primary *Wnt5a* knockout MEFs were stimulated with rWnt5a (0.2 μ g/mL) for 0, 1, or 6 hours, and the relative abundance of *Pdzn3* mRNA were determine by RT-qPCR. Error bars represent \pm SEM calculated from three technical replicates. t-test (unpaired) was performed to determine statistical significance for the following comparisons: 1hr vs. 0hr; 6hr vs. 0hr. P-values: * = $p < 0.05$, ** = $p < 0.01$, *** = $p < 0.001$.

Figure 3. A signaling cascade links non-canonical Wnt5a-Ror signaling to Pdzn3 degradation. A)

Representative histogram showing the effect of rWnt5a treatment on NIH/3T3 GFP-Pdzn3 (WRP) reporter cells. WRP cells were treated with rWnt5a (0.2 μ g/mL) for 6 hours, and GFP-Pdzn3 fluorescence was measured by flow cytometry. **B**) Dose-response curve showing GFP-Pdzn3 downregulation as a function of rWnt5a concentration in the WRP reporter assay. An EC_{50} of 77.1ng/mL was calculated. **C**) Histograms showing the effect of proteasome inhibitor (epoxomicin, 10 μ M), ubiquitin E1 inhibitor (PYR41, 10 μ M) and Cullin inhibitor (MLN4924, 10 μ M) on rWnt5a-induced Pdzn3 downregulation in the WRP reporter cells. Error bars represent \pm SEM calculated from three technical replicates. t-test (unpaired) was performed to determine statistical significance for the following comparisons: inhibitors vs. the vehicle control DMSO. **D**) Histograms showing the effect of canonical Wnt inhibitors, Dkk-1 (2 μ g/ μ L) and IWR-1-endo (10 μ M) on rWnt5a-induced Pdzn3 degradation in the WRP reporter cells. Error bars represent \pm SEM calculated from three technical replicates. t-test (unpaired) was performed to determine statistical significance for the following comparisons: inhibitors vs. the vehicle control DMSO. **E**) Histograms showing the effects of Fzd1, Fzd2 and Fzd7 overexpression on the median fluorescence of WRP reporter cells. Error bars represent \pm SEM calculated from two cell lines and three technical replicates per line. t-test (unpaired) was performed to determine statistical significance for the following comparisons: Fzd overexpression vs. the Myc epitope tag overexpression. **F**) Histograms showing the effects of DVL1, DVL2 and DVL3 overexpression on the median fluorescence of WRP reporter cells. Error bars represent \pm SEM calculated from two cell lines and three technical replicates per line. t-test (unpaired) was performed to determine statistical significance for the following comparisons: DVL

overexpression vs. the Myc epitope tag overexpression. **G)** Histograms showing the effect of CK1 inhibitor (D4476, 100 μ M) and GSK inhibitor (CHIR99021, 100 μ M) on rWnt5a-induced Pdzrn3 downregulation in the WRP reporter cells. Error bars represent \pm SEM calculated from three technical replicates. t-test (unpaired) was performed to determine statistical significance for the following comparisons: inhibitors vs. the vehicle control DMSO. **H)** Histograms showing the effects of genetically ablating *Kif26a* and *Kif26b* on rWnt5a-induced GFP-Pdzrn3 reporter degradation. Error bars represent \pm SEM calculated from three technical replicates. t-test (unpaired) was performed to determine statistical significance for the following comparisons: GFP-Pdzrn3 reporter in *Kif26a/Kif26b* double KO cells vs. GFP-Pdzrn3 reporter in WT cells. **I)** Histograms showing the effects of genetically ablating *Pdzrn3* and *Pdzrn4* on rWnt5a-induced GFP-Kif26b reporter (WRK) degradation. Error bars represent \pm SEM calculated from three technical replicates per line. t-test (unpaired) was performed to determine statistical significance for the following comparisons: GFP-Kif26b reporter in *Pdzrn3/Pdzrn4* double KO cells vs. GFP-Kif26b reporter in WT cells. P-values: * = $p < 0.05$, ** = $p < 0.01$, *** = $p < 0.001$.

Figure 3 Supplement. CRISPR/Cas9 mediated genetic deletions of *Kif26a*, *Pdzrn3*, and *Lnx4*. Reference sequences for *Kif26a* (A), *Pdzrn3* (B), and *Lnx4* (C) aligned to mutant alleles generated via targeting with short guide RNAs (sgRNAs) (underlined in reference, green sequence is PAM sequence) unique to each gene. Multiple deep sequencing results indicate that *Lnx4* is triploid, which is consistent with previous karyotyping of NIH/3T3 cells (Leibiger et al., 2013).

Figure 4. Phosphorylation of specific sites in the LNX3H domain is required for Wnt5a-dependent degradation of Pdzrn3 and related homologs.

A) Schematic of domains and identified phosphorylation sites of Pdzrn3. **B)** Histograms showing the effects of mutating Group 1 and Group 2 sites on Wnt5a-induced Pdzrn3 degradation. Error bars represent \pm SEM calculated from two cell lines and three technical replicates per line. t-test (unpaired) was performed to determine statistical significance for the following comparisons: mutant Pdzrn3 vs. WT Pdzrn3. **C)** Histograms showing the effects of mutating individual Group 2 sites on Wnt5a-induced Pdzrn3 degradation. Error bars represent \pm SEM calculated from two cell lines and three technical replicates per line. t-test (unpaired) was

performed to determine statistical significance for the following comparisons: mutant Pdzrn3 vs. WT Pdzrn3. **D)** Histograms showing the effects of Group 2 phosphomimetic mutations on Pdzrn3 reporter signals. Error bars represent \pm SEM calculated from two cell lines and three technical replicates per line. t-test (unpaired) was performed to determine statistical significance for the following comparisons: WT Pdzrn3 – vs + Wnt5a; phosphomimetic Pdzrn3 mutant vs. WT Pdzrn3 – and + Wnt5a; phosphomimetic Pdzrn3 mutant + Wnt5a vs. – Wnt5a. **E)** Schematic of Lnx family members and their conserved domains. Pdzrn3 is structurally most homologous to Lnx4. **F)** Alignment of a portion of the LNX3H domain shared by Pdzrn3, Lnx4, and Lnx5. The Pdzrn3 Group 2 phosphorylation sites identified through our MS screen are conserved (red stars and boxes). **G)** Histogram showing the effects of Wnt5a on the steady-state abundance of GFP-Lnx family member reporter cell lines. For clarity and ease of comparison across family members, the median reporter signal for the +Wnt5a condition was normalized to the –Wnt5a condition within the individual Lnx reporter. Error bars represent \pm SEM calculated from two (Lnx1, Lnx2, and Lnx5), four (Pdzrn3), or six (Lnx4) cell lines and three technical replicates per line. t-test (unpaired) was performed to determine statistical significance for the following comparisons: +Wnt5a vs. –Wnt5a for each Lnx family member. **H)** Histogram showing the effect of LNX3H truncation mutation on Pdzrn3 steady-state abundance. Error bars represent \pm SEM calculated from two (Pdzrn3 Δ LNX3H) or four (Pdzrn3) cell lines and three technical replicates per line. t-test (unpaired) was performed to determine statistical significance for the following comparisons: WT Pdzrn3 – vs + Wnt5a; Pdzrn3 Δ LNX3H –Wnt5a vs. WT Pdzrn3 –Wnt5a; Pdzrn3 Δ LNX3H +Wnt5a vs. –Wnt5a. **I)** Histogram showing the effect of LNX3H truncation mutation on Pdzrn4 steady-state abundance. Error bars represent \pm SEM calculated from two (Lnx4 Δ LNX3H) or six (Lnx4) cell lines and three technical replicates per line. t-test (unpaired) was performed to determine statistical significance for the following comparisons: WT Pdzrn4 – vs + Wnt5a; Pdzrn4 Δ LNX3H –Wnt5a vs. WT Pdzrn4 –Wnt5a; Pdzrn4 Δ LNX3H +Wnt5a vs. –Wnt5a. **J)** Model of Wnt5a-Ror-Pdzrn3 signaling. P-values: * = $p < 0.05$, ** = $p < 0.01$, *** = $p < 0.001$.

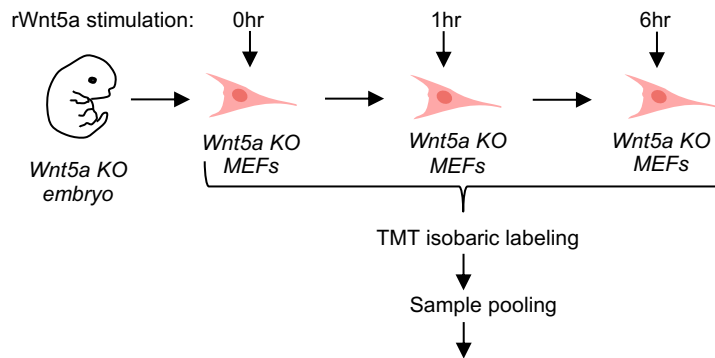
- AFZAL, A. R., RAJAB, A., FENSKE, C. D., OLDRIDGE, M., ELANKO, N., TERNES-PEREIRA, E., TUYSUZ, B., MURDAY, V. A., PATTON, M. A., WILKIE, A. O. & JEFFERY, S. 2000. Recessive Robinow syndrome, allelic to dominant brachydactyly type B, is caused by mutation of ROR2. *Nat Genet*, 25, 419-22.
- BAFICO, A., LIU, G., YANIV, A., GAZIT, A. & AARONSON, S. A. 2001. Novel mechanism of Wnt signalling inhibition mediated by Dickkopf-1 interaction with LRP6/Arrow. *Nat Cell Biol*, 3, 683-6.
- BAIZABAL, J. M., MISTRY, M., GARCIA, M. T., GOMEZ, N., OLUKOYA, O., TRAN, D., JOHNSON, M. B., WALSH, C. A. & HARWELL, C. C. 2018. The Epigenetic State of PRDM16-Regulated Enhancers in Radial Glia Controls Cortical Neuron Position. *Neuron*, 99, 239-241.
- BRYJA, V., SCHULTE, G. & ARENAS, E. 2007a. Wnt-3a utilizes a novel low dose and rapid pathway that does not require casein kinase 1-mediated phosphorylation of Dvl to activate beta-catenin. *Cell Signal*, 19, 610-6.
- BRYJA, V., SCHULTE, G., RAWAL, N., GRAHN, A. & ARENAS, E. 2007b. Wnt-5a induces Dishevelled phosphorylation and dopaminergic differentiation via a CK1-dependent mechanism. *J Cell Sci*, 120, 586-95.
- BUNN, K. J., DANIEL, P., ROSKEN, H. S., O'NEILL, A. C., CAMERON-CHRISTIE, S. R., MORGAN, T., BRUNNER, H. G., LAI, A., KUNST, H. P., MARKIE, D. M. & ROBERTSON, S. P. 2015. Mutations in DVL1 cause an osteosclerotic form of Robinow syndrome. *Am J Hum Genet*, 96, 623-30.
- CARVALLO, L., MUNOZ, R., BUSTOS, F., ESCOBEDO, N., CARRASCO, H., OLIVARES, G. & LARRAIN, J. 2010. Non-canonical Wnt signaling induces ubiquitination and degradation of Syndecan4. *J Biol Chem*, 285, 29546-55.
- CHOI, J., PARK, S. Y., COSTANTINI, F., JHO, E. H. & JOO, C. K. 2004. Adenomatous polyposis coli is down-regulated by the ubiquitin-proteasome pathway in a process facilitated by Axin. *J Biol Chem*, 279, 49188-98.
- CLEVERS, H. & NUSSE, R. 2012. Wnt/beta-catenin signaling and disease. *Cell*, 149, 1192-205.
- CONNACHER, M. K., TAY, J. W. & AHN, N. G. 2017. Rear-polarized Wnt5a-receptor-actin-myosin-polarity (WRAMP) structures promote the speed and persistence of directional cell migration. *Mol Biol Cell*, 28, 1924-1936.
- FLYNN, M., SAHA, O. & YOUNG, P. 2011. Molecular evolution of the LNX gene family. *BMC Evol Biol*, 11, 235.
- HIKASA, H., SHIBATA, M., HIRATANI, I. & TAIRA, M. 2002. The Xenopus receptor tyrosine kinase Xror2 modulates morphogenetic movements of the axial mesoderm and neuroectoderm via Wnt signaling. *Development*, 129, 5227-39.
- HO, H. Y., SUSMAN, M. W., BIKOFF, J. B., RYU, Y. K., JONAS, A. M., HU, L., KURUVILLA, R. & GREENBERG, M. E. 2012. Wnt5a-Ror-Dishevelled signaling constitutes a core developmental pathway that controls tissue morphogenesis. *Proc Natl Acad Sci U S A*, 109, 4044-51.
- HUANG, S. M., MISHINA, Y. M., LIU, S., CHEUNG, A., STEGMEIER, F., MICHAUD, G. A., CHARLAT, O., WIELLETTE, E., ZHANG, Y., WIESSNER, S., HILD, M., SHI, X., WILSON, C. J., MICKANIN, C., MYER, V., FAZAL, A., TOMLINSON, R., SERLUCA, F., SHAO, W., CHENG, H., SHULTZ, M., RAU, C., SCHIRLE, M., SCHLEGL, J., GHIDELLI, S., FAWELL, S., LU, C., CURTIS, D., KIRSCHNER, M. W., LENGAUER, C., FINAN, P. M., TALLARICO, J. A., BOUWMEESTER, T., PORTER, J. A., BAUER, A. & CONG, F. 2009. Tankyrase inhibition stabilizes axin and antagonizes Wnt signalling. *Nature*, 461, 614-20.
- KARUNA, E. P., SUSMAN, M. W. & HO, H. H. 2018. Quantitative Live-cell Reporter Assay for Noncanonical Wnt Activity. *Bio-protocol* 8, e2762.
- KIM, S. E., HUANG, H., ZHAO, M., ZHANG, X., ZHANG, A., SEMONOV, M. V., MACDONALD, B. T., ZHANG, X., GARCIA ABREU, J., PENG, L. & HE, X. 2013. Wnt stabilization of beta-catenin reveals principles for morphogen receptor-scaffold assemblies. *Science*, 340, 867-70.
- LEE, E., SALIC, A., KRUGER, R., HEINRICH, R. & KIRSCHNER, M. W. 2003. The roles of APC and Axin derived from experimental and theoretical analysis of the Wnt pathway. *PLoS Biol*, 1, E10.
- LEE, H. J., SHI, D. L. & ZHENG, J. J. 2015. Conformational change of Dishevelled plays a key regulatory role in the Wnt signaling pathways. *Elife*, 4, e08142.

- LEIBIGER, C., KOSYAKOVA, N., MKRTCHYAN, H., GLEI, M., TRIFONOV, V. & LIEHR, T. 2013. First molecular cytogenetic high resolution characterization of the NIH 3T3 cell line by murine multicolor banding. *J Histochem Cytochem*, 61, 306-12.
- LU, Z., JE, H. S., YOUNG, P., GROSS, J., LU, B. & FENG, G. 2007. Regulation of synaptic growth and maturation by a synapse-associated E3 ubiquitin ligase at the neuromuscular junction. *J Cell Biol*, 177, 1077-89.
- MANSOUR, T. A., LUCOT, K., KONOPELSKI, S. E., DICKINSON, P. J., STURGES, B. K., VERNAU, K. L., CHOI, S., STERN, J. A., THOMASY, S. M., DORING, S., VERSTRAETE, F. J. M., JOHNSON, E. G., YORK, D., REBHUN, R. B., HO, H. H., BROWN, C. T. & BANNASCH, D. L. 2018. Whole genome variant association across 100 dogs identifies a frame shift mutation in DISHEVELLED 2 which contributes to Robinow-like syndrome in Bulldogs and related screw tail dog breeds. *PLoS Genet*, 14, e1007850.
- MCALISTER, G. C., NUSINOW, D. P., JEDRYCHOWSKI, M. P., WUHR, M., HUTTLIN, E. L., ERICKSON, B. K., RAD, R., HAAS, W. & GYGI, S. P. 2014. MultiNotch MS3 enables accurate, sensitive, and multiplexed detection of differential expression across cancer cell line proteomes. *Anal Chem*, 86, 7150-8.
- MENG, L., MOHAN, R., KWOK, B. H., ELOFSSON, M., SIN, N. & CREWS, C. M. 1999. Epoxomicin, a potent and selective proteasome inhibitor, exhibits in vivo antiinflammatory activity. *Proc Natl Acad Sci U S A*, 96, 10403-8.
- MOON, R. T., CAMPBELL, R. M., CHRISTIAN, J. L., MCGREW, L. L., SHIH, J. & FRASER, S. 1993. Xwnt-5A: a maternal Wnt that affects morphogenetic movements after overexpression in embryos of *Xenopus laevis*. *Development*, 119, 97-111.
- NOMI, M., OISHI, I., KANI, S., SUZUKI, H., MATSUDA, T., YODA, A., KITAMURA, M., ITOH, K., TAKEUCHI, S., TAKEDA, K., AKIRA, S., IKEYA, M., TAKADA, S. & MINAMI, Y. 2001. Loss of mRor1 enhances the heart and skeletal abnormalities in mRor2-deficient mice: redundant and pleiotropic functions of mRor1 and mRor2 receptor tyrosine kinases. *Mol Cell Biol*, 21, 8329-35.
- NUSSE, R. & VARMUS, H. 2012. Three decades of Wnts: a personal perspective on how a scientific field developed. *EMBO J*, 31, 2670-84.
- PAPKOFF, J., RUBINFELD, B., SCHRYVER, B. & POLAKIS, P. 1996. Wnt-1 regulates free pools of catenins and stabilizes APC-catenin complexes. *Mol Cell Biol*, 16, 2128-34.
- PARK, H. W., KIM, Y. C., YU, B., MOROISHI, T., MO, J. S., PLOUFFE, S. W., MENG, Z., LIN, K. C., YU, F. X., ALEXANDER, C. M., WANG, C. Y. & GUAN, K. L. 2015. Alternative Wnt Signaling Activates YAP/TAZ. *Cell*, 162, 780-94.
- PAULO, J. A., MCALISTER, F. E., EVERLEY, R. A., BEAUSOLEIL, S. A., BANKS, A. S. & GYGI, S. P. 2015. Effects of MEK inhibitors GSK1120212 and PD0325901 in vivo using 10-plex quantitative proteomics and phosphoproteomics. *Proteomics*, 15, 462-73.
- PERSON, A. D., BEIRAGHI, S., SIEBEN, C. M., HERMANSON, S., NEUMANN, A. N., ROBU, M. E., SCHLEIFFARTH, J. R., BILLINGTON, C. J., JR., VAN BOKHOVEN, H., HOOGEBOOM, J. M., MAZZEU, J. F., PETRYK, A., SCHIMMENTI, L. A., BRUNNER, H. G., EKKER, S. C. & LOHR, J. L. 2010. WNT5A mutations in patients with autosomal dominant Robinow syndrome. *Dev Dyn*, 239, 327-37.
- QI, J., LEE, H. J., SAQUET, A., CHENG, X. N., SHAO, M., ZHENG, J. J. & SHI, D. L. 2017. Autoinhibition of Dishevelled protein regulated by its extreme C terminus plays a distinct role in Wnt/beta-catenin and Wnt/planar cell polarity (PCP) signaling pathways. *J Biol Chem*, 292, 5898-5908.
- RAN, F. A., HSU, P. D., LIN, C. Y., GOOTENBERG, J. S., KONERMANN, S., TREVINO, A. E., SCOTT, D. A., INOUE, A., MATOBA, S., ZHANG, Y. & ZHANG, F. 2013. Double nicking by RNA-guided CRISPR Cas9 for enhanced genome editing specificity. *Cell*, 154, 1380-9.
- SEWDUTH, R. N., JASPARD-VINASSA, B., PEGHAIRE, C., GUILLABERT, A., FRANZL, N., LARRIEU-LAHARGUE, F., MOREAU, C., FRUTTIGER, M., DUFOURCQ, P., COUFFINHAL, T. & DUPLAA, C. 2014. The ubiquitin ligase PDZRN3 is required for vascular morphogenesis through Wnt/planar cell polarity signalling. *Nat Commun*, 5, 4832.
- STEINHART, Z. & ANGERS, S. 2018. Wnt signaling in development and tissue homeostasis. *Development*, 145.

- SUSMAN, M. W., KARUNA, E. P., KUNZ, R. C., GUJRAL, T. S., CANTU, A. V., CHOI, S. S., JONG, B. Y., OKADA, K., SCALES, M. K., HUM, J., HU, L. S., KIRSCHNER, M. W., NISHINAKAMURA, R., YAMADA, S., LAIRD, D. J., JAO, L. E., GYGI, S. P., GREENBERG, M. E. & HO, H. H. 2017. Kinesin superfamily protein Kif26b links Wnt5a-Ror signaling to the control of cell and tissue behaviors in vertebrates. *Elife*, 6.
- TING, L., RAD, R., GYGI, S. P. & HAAS, W. 2011. MS3 eliminates ratio distortion in isobaric multiplexed quantitative proteomics. *Nat Methods*, 8, 937-40.
- TONG, S., SI, Y., YU, H., ZHANG, L., XIE, P. & JIANG, W. 2017. MLN4924 (Pevonedistat), a protein neddylation inhibitor, suppresses proliferation and migration of human clear cell renal cell carcinoma. *Sci Rep*, 7, 5599.
- UCHIYAMA, Y., SAKAGUCHI, M., TERABAYASHI, T., INENAGA, T., INOUE, S., KOBAYASHI, C., OSHIMA, N., KIYONARI, H., NAKAGATA, N., SATO, Y., SEKIGUCHI, K., MIKI, H., ARAKI, E., FUJIMURA, S., TANAKA, S. S. & NISHINAKAMURA, R. 2010. Kif26b, a kinesin family gene, regulates adhesion of the embryonic kidney mesenchyme. *Proc Natl Acad Sci U S A*, 107, 9240-5.
- VEEMAN, M. T., AXELROD, J. D. & MOON, R. T. 2003. A second canon. Functions and mechanisms of beta-catenin-independent Wnt signaling. *Dev Cell*, 5, 367-77.
- WHITE, J., MAZZEU, J. F., HOISCHEN, A., JHANGIANI, S. N., GAMBIN, T., ALCINO, M. C., PENNEY, S., SARAIVA, J. M., HOVE, H., SKOVBY, F., KAYSERILI, H., ESTRELLA, E., VULTO-VAN SILFHOUT, A. T., STEEHOUWER, M., MUZNY, D. M., SUTTON, V. R., GIBBS, R. A., BAYLOR-HOPKINS CENTER FOR MENDELIAN, G., LUPSKI, J. R., BRUNNER, H. G., VAN BON, B. W. & CARVALHO, C. M. 2015. DVL1 frameshift mutations clustering in the penultimate exon cause autosomal-dominant Robinow syndrome. *Am J Hum Genet*, 96, 612-22.
- WHITE, J. J., MAZZEU, J. F., COBAN-AKDEMIR, Z., BAYRAM, Y., BAHRAMBEIGI, V., HOISCHEN, A., VAN BON, B. W. M., GEZDIRICI, A., GULEC, E. Y., RAMOND, F., TOURAIN, R., THEVENON, J., SHINAWI, M., BEAVER, E., HEELEY, J., HOOVER-FONG, J., DURMAZ, C. D., KARABULUT, H. G., MARZIOGLU-OZDEMIR, E., CAYIR, A., DUZ, M. B., SEVEN, M., PRICE, S., FERREIRA, B. M., VIANNA-MORGANTE, A. M., ELLARD, S., PARRISH, A., STALS, K., FLORES-DABOUB, J., JHANGIANI, S. N., GIBBS, R. A., BAYLOR-HOPKINS CENTER FOR MENDELIAN, G., BRUNNER, H. G., SUTTON, V. R., LUPSKI, J. R. & CARVALHO, C. M. B. 2018. WNT Signaling Perturbations Underlie the Genetic Heterogeneity of Robinow Syndrome. *Am J Hum Genet*, 102, 27-43.
- WHITE, J. J., MAZZEU, J. F., HOISCHEN, A., BAYRAM, Y., WITHERS, M., GEZDIRICI, A., KIMONIS, V., STEEHOUWER, M., JHANGIANI, S. N., MUZNY, D. M., GIBBS, R. A., BAYLOR-HOPKINS CENTER FOR MENDELIAN, G., VAN BON, B. W. M., SUTTON, V. R., LUPSKI, J. R., BRUNNER, H. G. & CARVALHO, C. M. B. 2016. DVL3 Alleles Resulting in a -1 Frameshift of the Last Exon Mediate Autosomal-Dominant Robinow Syndrome. *Am J Hum Genet*, 98, 553-561.
- WITZE, E. S., CONNACHER, M. K., HOUEL, S., SCHWARTZ, M. P., MORPHEW, M. K., REID, L., SACKS, D. B., ANSETH, K. S. & AHN, N. G. 2013. Wnt5a directs polarized calcium gradients by recruiting cortical endoplasmic reticulum to the cell trailing edge. *Dev Cell*, 26, 645-57.
- WITZE, E. S., LITMAN, E. S., ARGAST, G. M., MOON, R. T. & AHN, N. G. 2008. Wnt5a control of cell polarity and directional movement by polarized redistribution of adhesion receptors. *Science*, 320, 365-9.
- YAMAGUCHI, T. P., BRADLEY, A., MCMAHON, A. P. & JONES, S. 1999. A Wnt5a pathway underlies outgrowth of multiple structures in the vertebrate embryo. *Development*, 126, 1211-23.
- YANG, Y., KITAGAKI, J., DAI, R. M., TSAI, Y. C., LORICK, K. L., LUDWIG, R. L., PIERRE, S. A., JENSEN, J. P., DAVYDOV, I. V., OBEROI, P., LI, C. C., KENTEN, J. H., BEUTLER, J. A., VOUSDEN, K. H. & WEISSMAN, A. M. 2007. Inhibitors of ubiquitin-activating enzyme (E1), a new class of potential cancer therapeutics. *Cancer Res*, 67, 9472-81.

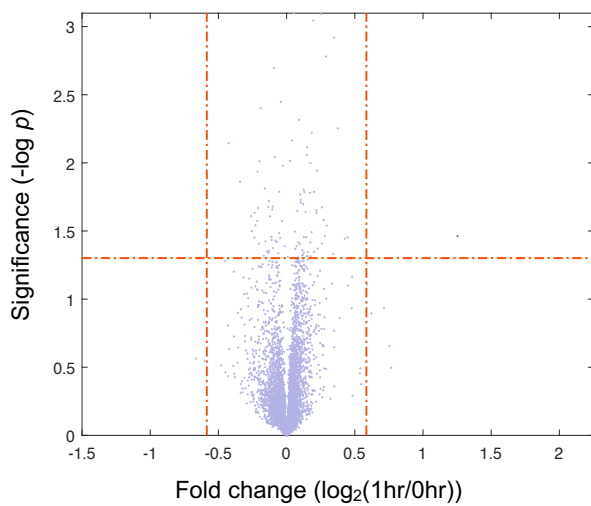
Figure 1

A

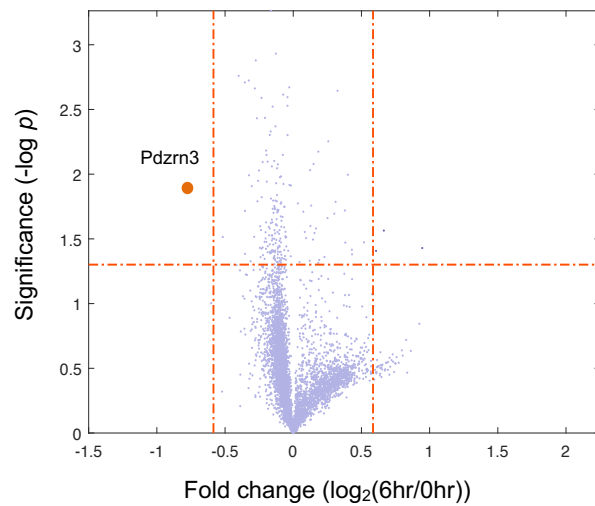


LC/MS3 tryptic/phospho-tryptic peptide identification and quantification

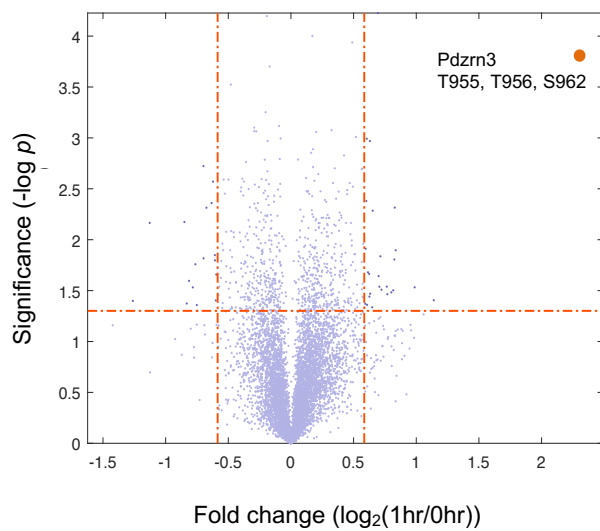
B



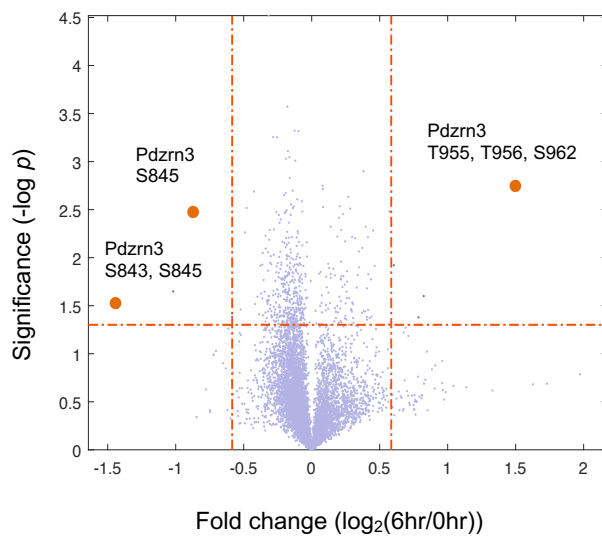
C



D



E



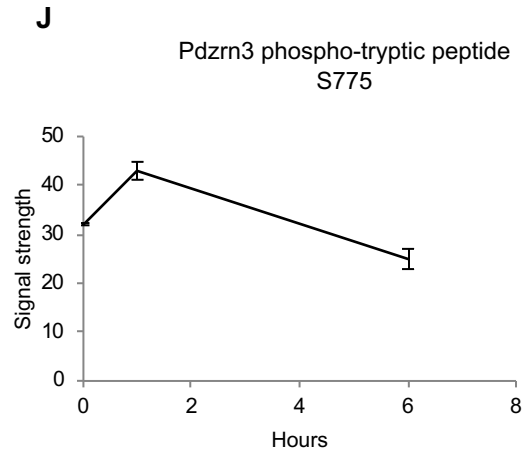
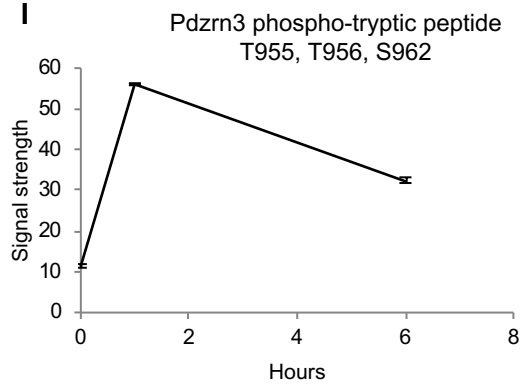
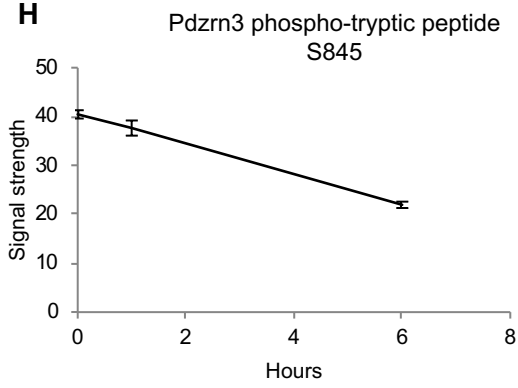
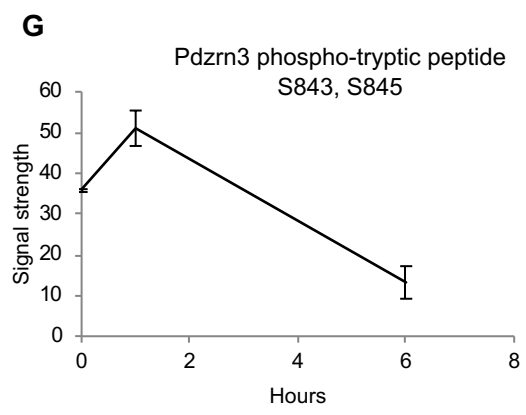
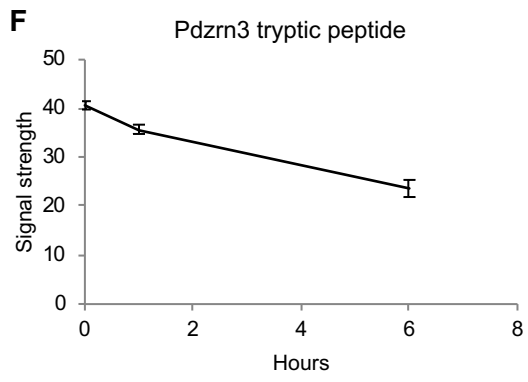
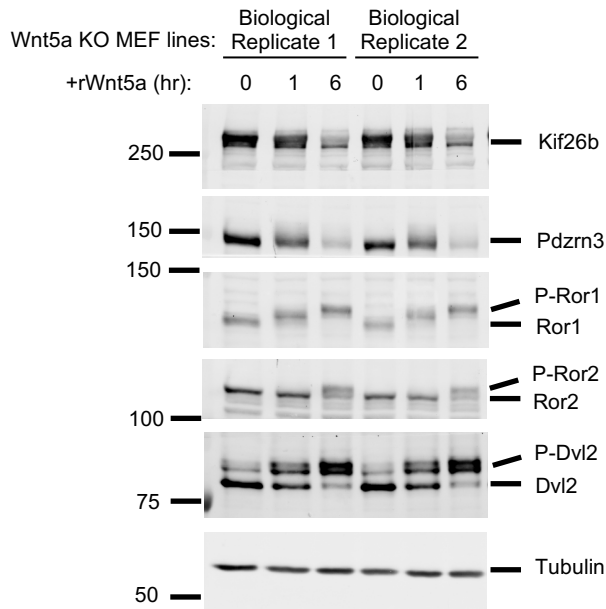
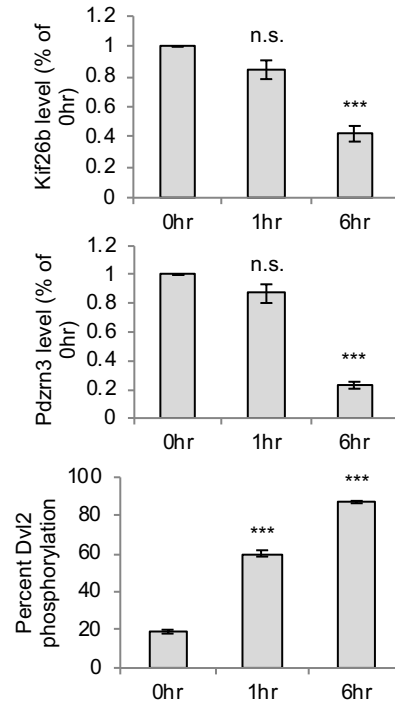
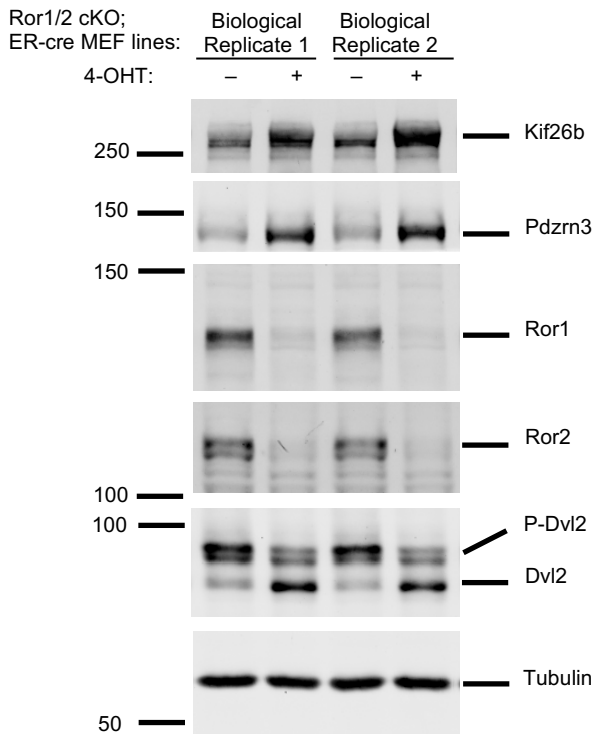
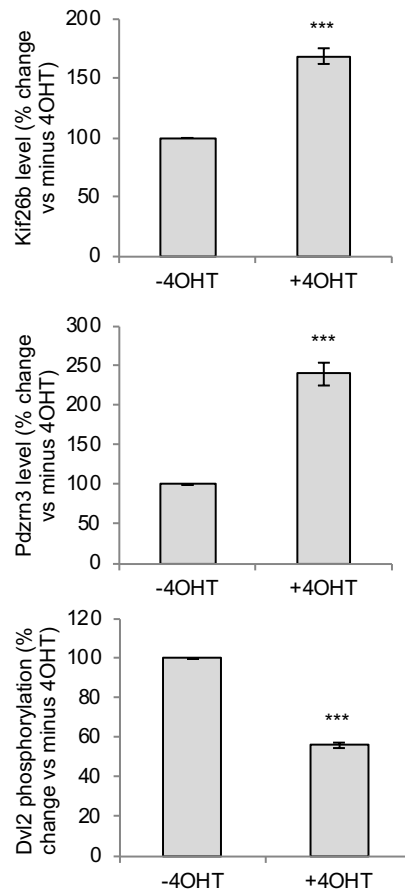


Figure 2**A****B****C****D**

E

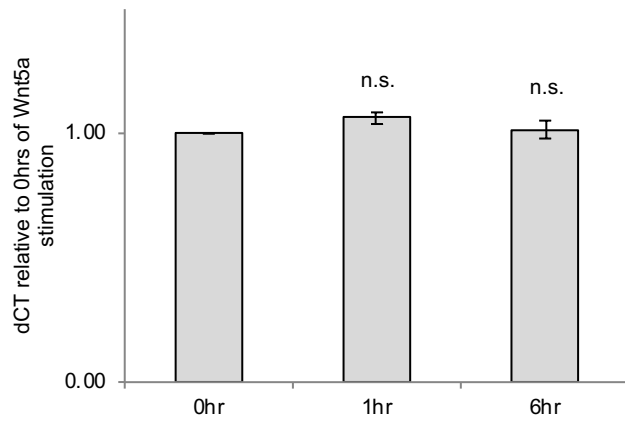
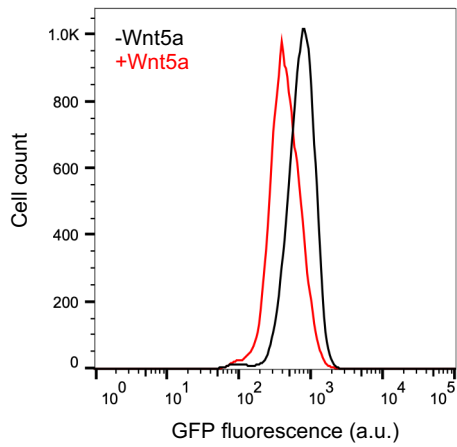
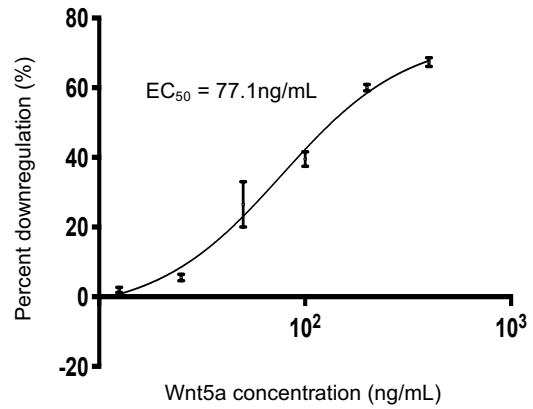
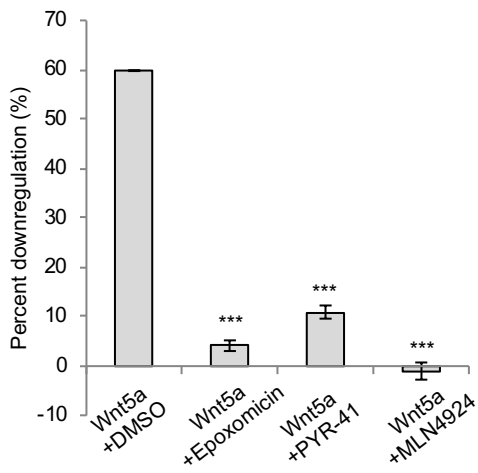
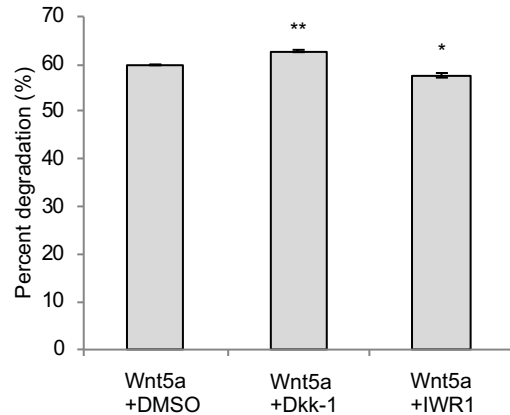
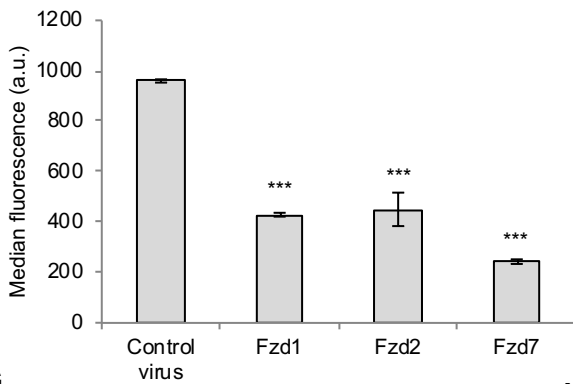
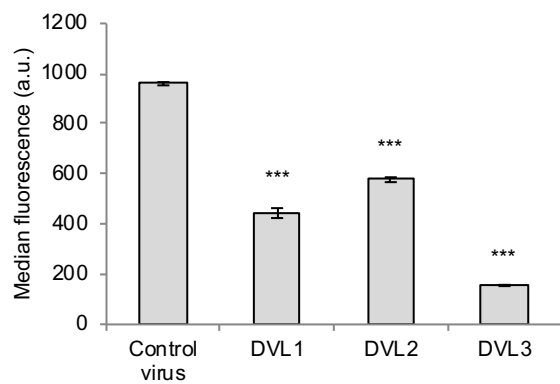
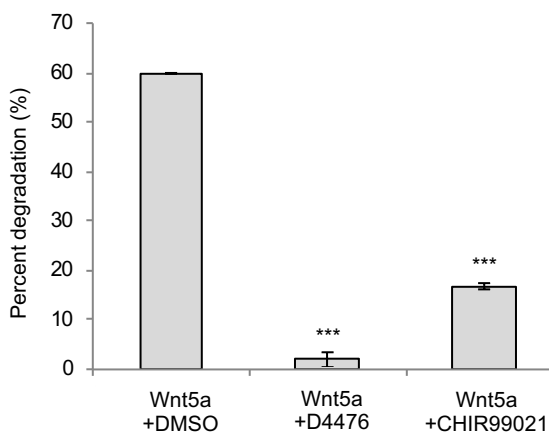
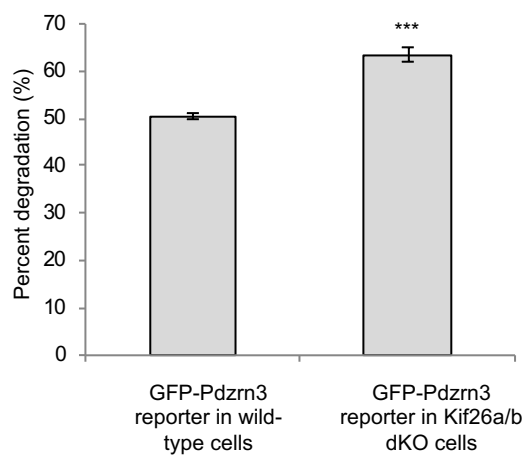


Figure 3**A****B****C****D****E****F****G****H**

I

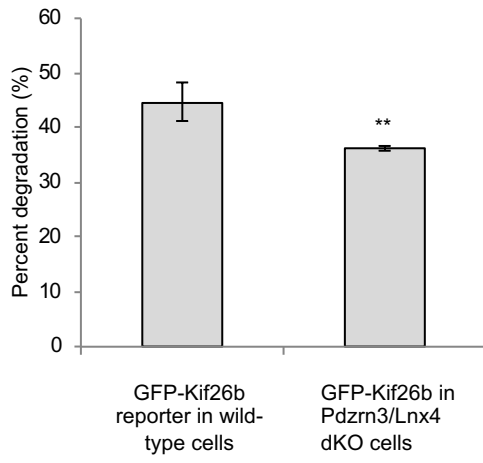


Figure 3 Supplement

A

```
Kif26a reference      CTGCCACACGAAGCTCGTGGAGCTAAAACGACAGGCGTGGAAGTTGGTCAGCG
Mutant allele 1      ctgccacacgaagctcg-----tgggaagttggtcagcg (-20)
Mutant allele 2      ctgccacacgaa-----gtggcgtggaagttggtcagcg (-19)
```

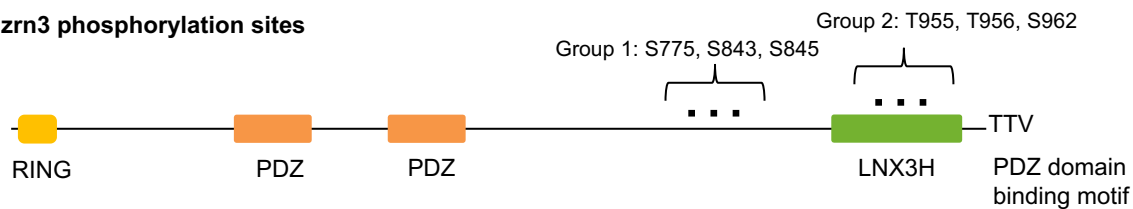
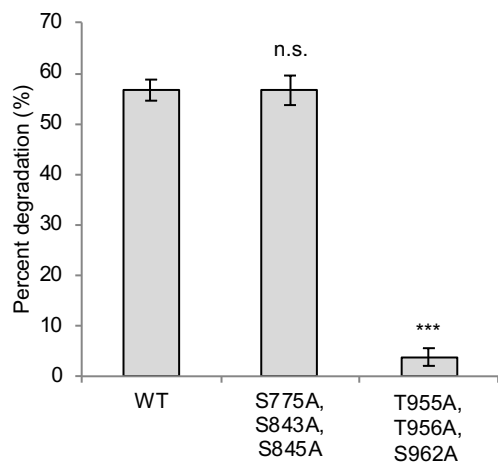
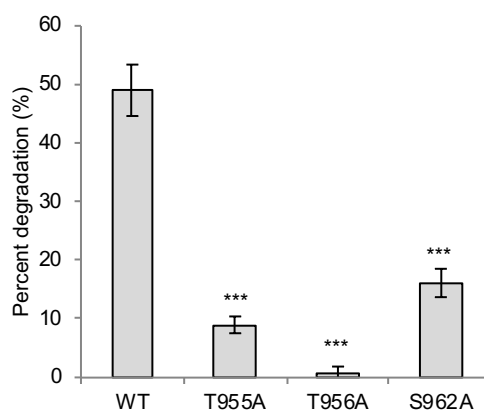
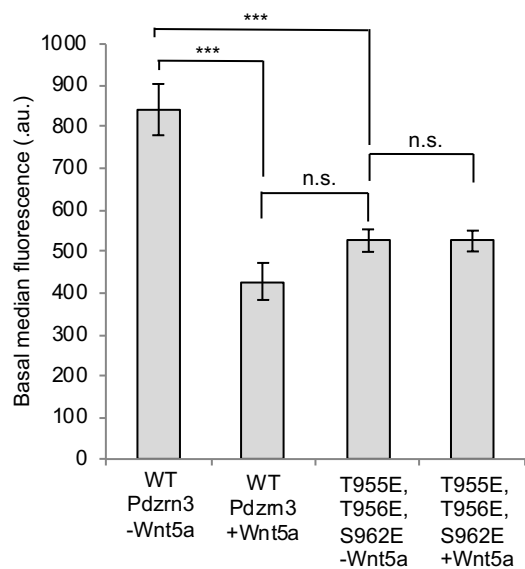
B

```
Pdzn3 reference      GGGCAGCTGCCCCGCGCGTTGTCGCGTTCGCCTATCGGCCAAGGAGCTCAAC
Mutant allele 1      ggcagctgccccgcgc-----ggtcgcctgtcgccaaggagctcaac (-8)

Pdzn3 reference      GGGCAGCTGCCCCGCGCGTTGTC-----GCGTTCGCCTATCGGCCAAGGA
Mutant allele 2      GGGCAGCTGCCCCGcgactacccaggtcgcctggtcgcctgtcgccaaggA (+8)
```

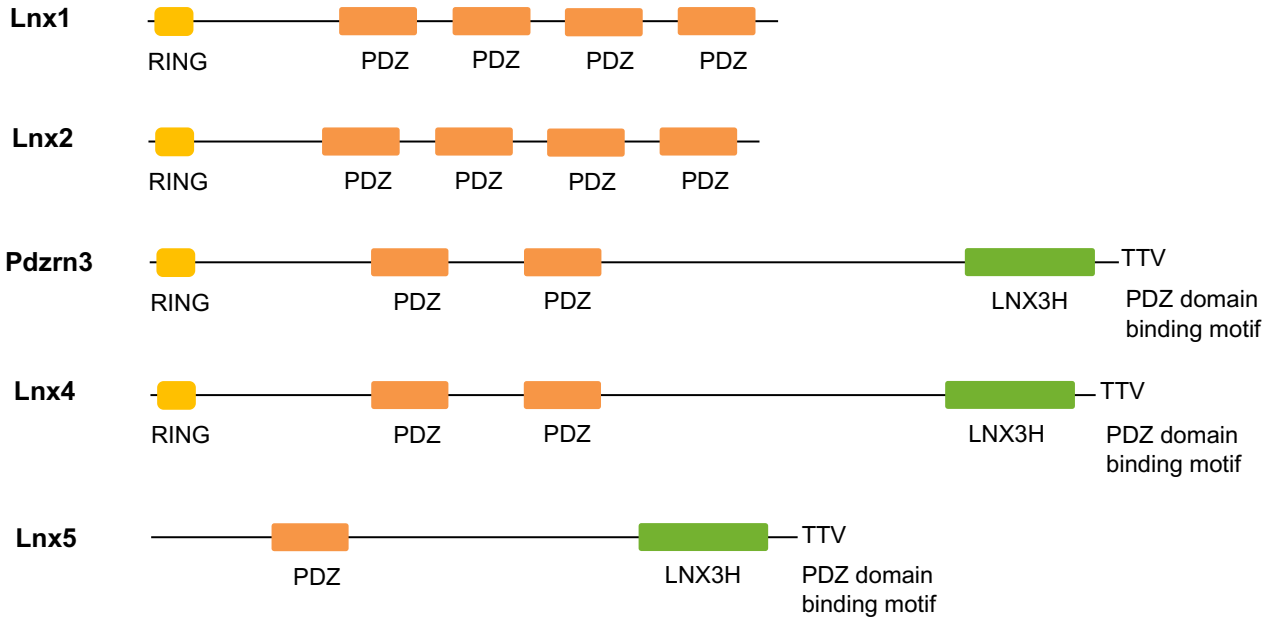
C

```
LnX4 reference      GCGGACTCCCTCAGCCGCCAACATACGGCATGACTCCGGAAGTACAGCTCACGAATGCCAGCACACA
Mutant allele 1      ggcggactcccctcagccgtatgt-----tggccggctcacgaatgccagcacaca (-19)
Mutant allele 2      ggcggactcccctcag-----ccggccaaca (-44)
Mutant allele 3      ggcggactcccctcag-----ccggaagtacagctcacgaatgccagcacaca (-22)
```


Figure 4**A****Pdzn3 phosphorylation sites****B****C****D**

E

The Lnx/Pdzrn family



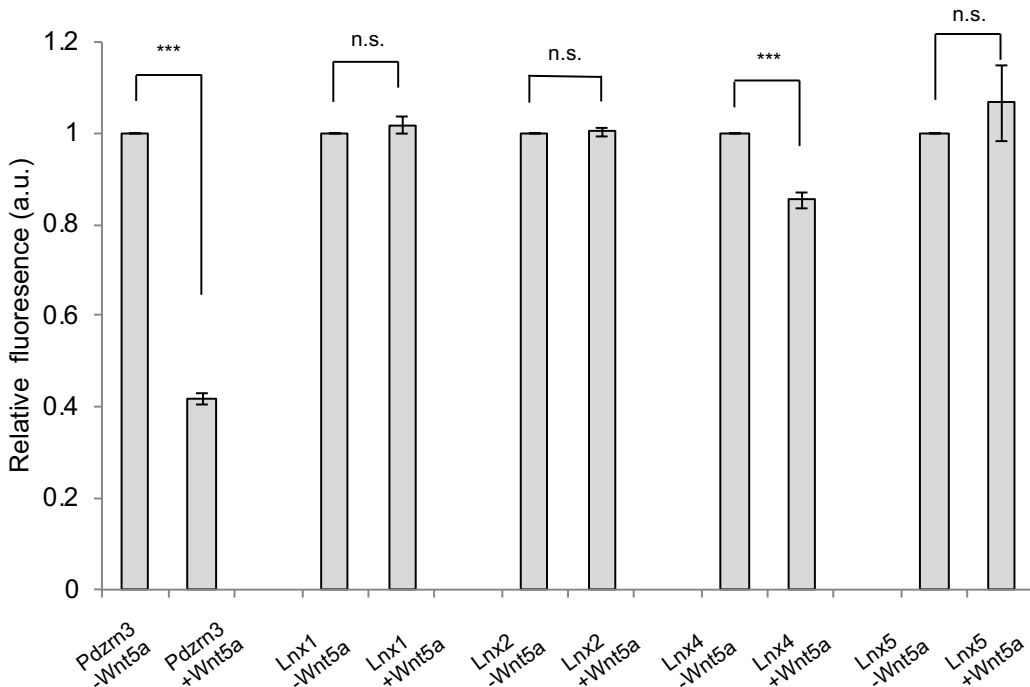
F

LNX3H domain homology

Group 2

Lnx5 RYVAKRPVRDRLLKARALKIREERSGM**T**DDDAVSEMKGGRYWSKEERKQHLIRAREQRK
Pdzrn3 RYITKRPVRDRLLRERALKIREERSGM**T**DDDAVSEMKGGRYWSKEERKQHLVKAKEQRR
Lnx4 RYITKRPVRDRILKERALKIKEERSGM**T**DDDTMSEMKGGRYWSKEERKQHLVRAKEQRR
** : : ***** : * : ***** : ***** : : ***** : ***** : : * : ** :

G



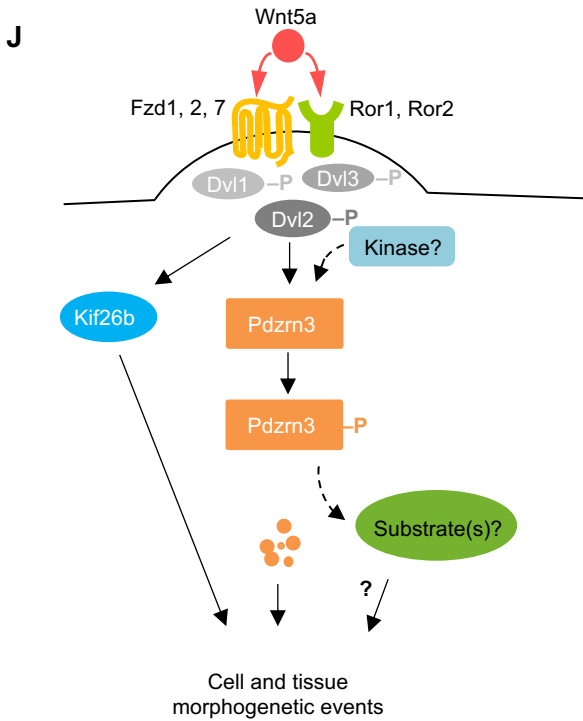
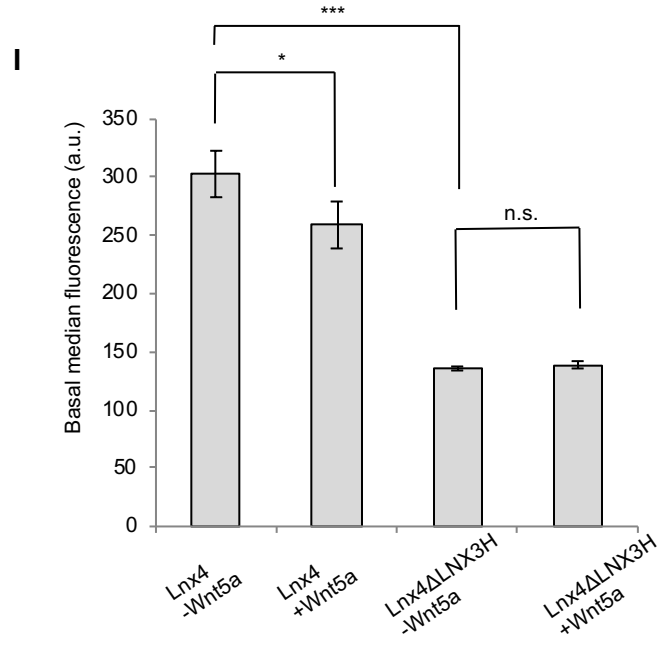
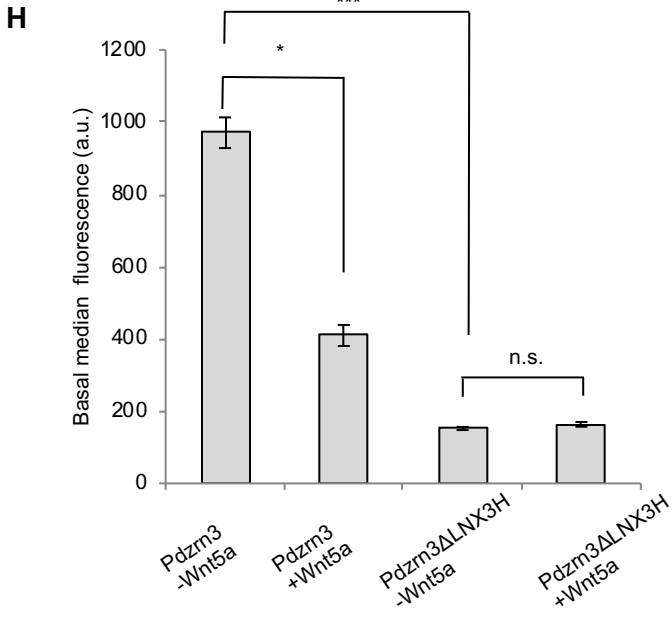


Table 1 - Hits from Wnt5a knockout MEF TMT/MS3 screen
Protein abundance changes after 1 hour of rWnt5a stimulation

upregulated

Gene symbol	Protein description	Fold change	p (<0.05)	>1.5-fold change
Egr1	Early growth response protein	2.38439693	0.034497	

No genes upregulated with a >1.4-fold change

downregulated

Gene symbol	Protein description	Fold change	p (<0.05)	>1.5-fold change
-------------	---------------------	-------------	-----------	------------------

No genes downregulated with a >1.5-fold change

No genes downregulated with a >1.4-fold change

Protein abundance changes after 6 hours of rWnt5a stimulation

upregulated

Gene symbol	Protein description	Fold change	p (<0.05)	>1.5-fold change
Wnt5a	Isoform 2 of Protein Wnt-5a	1.92657207	0.037231	
Tomm20	Mitochondrial import receptor subunit	1.58488672	0.027277	
Mgst3	Microsomal glutathione S-transferase 3	1.52325576	0.039168	
ORF3	UPF0480 protein	1.43262102	0.033593	>1.4-fold change

downregulated

Gene symbol	Protein description	Fold change	p (<0.05)	>1.5-fold change
Pdzn3	Isoform 2 of E3 ubiquitin-protein ligase PDZRN3	-1.7213491	0.012706	
Pex19	Peroxisomal biogenesis factor 19	-1.4307244	0.030568	>1.4-fold change

Phosphopeptides after 1 hour of rWnt5a stimulation

upregulated

Gene symbol	Protein description	Fold change	p (<0.05)	>1.5-fold change
Pdzn3	Isoform 2 of E3 ubiquitin-protein ligase PDZRN3	4.89634836	0.000145	

Cttnbp2nl	CTTNBP2 N-terminal-like protein	2.20373642	0.039309
Fam193a	Protein FAM193A	1.98184441	0.029347
Cttnbp2nl	CTTNBP2 N-terminal-like protein	1.78868644	0.049764
Smad5	Mothers against decapentaplegic homolog 5	1.78489033	0.012698
Ppm1g	Protein phosphatase 1G	1.77555122	0.00484
Myo9b	Uncharacterized protein	1.77168825	0.015636
Trim28	Transcription intermediary factor 1-beta	1.76072021	0.031412
Ythdf2	Uncharacterized protein	1.74208623	0.032915
Pitpnb	Phosphatidylinositol transfer protein beta isoform	1.70467017	0.034315
Runx2	Isoform 2 of Runt-related transcription factor 2	1.69891043	0.02888
Golga4	Golgin subfamily A member 4	1.64988603	0.030965
Wiz	Isoform S of Protein Wiz	1.64010503	0.014559
Jmy	Isoform 3 of Junction-mediating and -regulatory protei	1.63159317	0.028972
Ccs	Copper chaperone for superoxide dismutase	1.62410293	0.022787
Znf516	Zinc finger protein 516	1.61724029	5.93E-05
Cit	Isoform 3 of Citron Rho-interacting kinase	1.57217286	0.005184
Pfkfb3	6-phosphofructo-2-kinase/fructose-2,6-biphosphatase	1.56721303	0.046131
Cbl	E3 ubiquitin-protein ligase CBL	1.55046765	0.033896
Nhsl1	Isoform 3 of NHS-like protein 1	1.54778574	0.001073
-	Uncharacterized protein FLJ45252 homolog	1.54340103	0.036225

	Uncharacterized protein			
Svil		1.54143915	0.02169	
Sos1	Son of sevenless homolog 1	1.53135359	0.020893	
Plcg1	1-phosphatidylinositol-4,5-bisphosphate phosphodiesterase gamma-1	1.52348015	0.04368	
Pfkfb3	6-phosphofructo-2-kinase/fructose-2,6-biphosphatase	1.52089246	0.001019	
Ppfibp1	Isoform 3 of Liprin-beta-1	1.51729378	0.004173	
Ptpn11	Isoform 2 of Tyrosine-protein phosphatase non-receptor type 11	1.51187355	0.01227	
Nhsl1	Isoform 3 of NHS-like protein 1	1.50814819	0.0426	
Myc	Myc proto-oncogene protein	1.4912389	0.01099	>1.4-fold change
Lmo7	Uncharacterized protein	1.48729622	0.027091	
Cald1	Uncharacterized protein	1.48701178	0.036531	
Dvl2	Segment polarity protein dishevelled homolog DVL-2	1.48086717	0.002012	
Nf1	Isoform 1 of Neurofibromin	1.48075369	0.030678	
Fer	Isoform 2 of Tyrosine-protein kinase Fer	1.48039856	0.016535	
Nup98	Uncharacterized protein	1.46133083	0.042083	
Rpl29	60S ribosomal protein L29	1.44329047	0.046032	
Abl1	Isoform IV of Tyrosine-protein kinase ABL1	1.44161993	0.027651	
Maged1	Melanoma-associated antigen D1	1.43997197	0.039443	
Ccnl1	Cyclin-L1	1.43229825	0.00098	
Ndrp1	Protein NDRG1	1.42850036	0.020054	
Golga4	Isoform 2 of Golgin subfamily A member 4	1.42700633	0.047654	
Clasp1	Uncharacterized protein	1.42585101	0.013897	

Eps15l1	Isoform 2 of Epidermal growth factor receptor substrate 15-like 1	1.41925481	0.013828
Rin3	Ras and Rab interactor 3	1.41280026	0.033785
Arhgap28	Isoform 2 of Rho GTPase-activating protein 28	1.40860678	0.00301
E2f7	Transcription factor E2F7	1.40787996	0.016597
Fam21	WASH complex subunit FAM21	1.40421895	0.000116

downregulated

Gene symbol	Protein description	Fold change	p (<0.05)	>1.5-fold change
Marcks	Myristoylated alanine-rich C-kinase substrate	-2.3973859	0.039918	
Nolc1	Uncharacterized protein	-2.1844007	0.006836	
Ahnak	Uncharacterized protein	-1.8026613	0.006695	
Ahnak	Uncharacterized protein	-1.7797038	0.042335	
Cald1	Uncharacterized protein	-1.7570389	0.025368	
Marcks	Myristoylated alanine-rich C-kinase substrate	-1.720977	0.029386	
Kif26b	Kinesin-like protein KIF26B	-1.6966715	0.017427	
Anln	Actin-binding protein anillin	-1.6833907	0.043808	
Mcm4	DNA replication licensing factor MCM4	-1.6224145	0.001891	
-	Uncharacterized protein C1orf198 homolog	-1.6214208	0.015245	
Irf2bpl	Interferon regulatory factor 2-binding protein-like	-1.5960168	0.00485	
Nufip2	Nuclear fragile X mental retardation-interacting protein 2	-1.5511997	0.004365	
Map2	Microtubule-associated protein 2	-1.5388129	0.002688	

Zc3hc1	Isoform 2 of Nuclear-interacting partner of ALK	-1.5232583	0.01419	
Nufip2	Nuclear fragile X mental retardation-interacting protein 2	-1.5224691	0.015971	
Ssfa2	Sperm-specific antigen 2 homolog	-1.5155006	0.039513	
Cald1	Uncharacterized protein	-1.5118212	0.021995	
Sdpr	Serum deprivation-response protein	-1.4930308	0.03501	>1.4-fold change
Ncapd2	Isoform 2 of Condensin complex subunit 1	-1.4861123	0.028937	
Ezh2	Isoform ENX-1B of Histone-lysine N-methyltransferase EZH2	-1.4738262	0.023732	
Cep170	Centrosomal protein of 170 kD	-1.4699737	0.016189	
Zc3hc1	Isoform 2 of Nuclear-interacting partner of ALK	-1.4617502	0.046771	
Osbpl11	Oxysterol-binding protein-related protein 11	-1.461438	0.010918	
Cep170	Centrosomal protein of 170 kD	-1.4584582	0.041928	
Ankrd11	Uncharacterized protein	-1.4547921	0.012658	
Aak1	Isoform 2 of AP2-associated protein kinase 1	-1.4509981	0.002565	
Plec	Isoform PLEC-1A of Plectin	-1.4417757	0.003531	
Rab11fip5	MKIAA0857 protein (Fragment)	-1.4327951	0.025892	
Larp1	La-related protein 1	-1.4305745	0.008354	
Map1b	Microtubule-associated protein 1	-1.4303788	0.018224	
Lasp1	LIM and SH3 domain protein 1	-1.4124158	0.002568	
Sorbs1	Uncharacterized protein	-1.4105315	0.030254	
R3hdm1	R3hdm1 protein	-1.4029545	0.036937	
Nolc1	Uncharacterized protein	-1.4000489	0.026646	

Phosphopeptides after 6 hours of rWnt5a stimulation

upregulated

Gene symbol	Protein description	Fold change	p (<0.05)	>1.5-fold change
Pdzn3	Isoform 2 of E3 ubiquitin-protein ligase PDZRN3	2.83867605	0.001695	
Snip3l	BCL2/adenovirus E1B 19 kDa protein-interacting protein 3-like	1.76999942	0.025135	
Fndc3a	Fibronectin type III domain-containing protein	1.72367539	0.04181	
Csnk1g3	Casein kinase I isoform gamma-3	1.51977428	0.011998	

Dvl2	Segment polarity protein dishevelled homolog DVL-2	1.4882145	0.003304	>1.4-fold change
Mia3	Isoform 3 of Melanoma inhibitory activity protein 3	1.48109347	0.049233	

downregulated

Gene symbol	Protein description	Fold change	p (<0.05)	>1.5-fold change
Pdzn3	Isoform 2 of E3 ubiquitin-protein ligase PDZRN3	-2.7174416	0.030081	
Kif26b	Kinesin-like protein KIF26B	-2.0259939	0.022447	
Pdzn3	Isoform 2 of E3 ubiquitin-protein ligase PDZRN3	-1.8443701	0.003328	
-	UPF0690 protein C1orf52 homolog	-1.5001226	0.041414	

Pebp1	Phosphatidylethanolamine-binding protein 1	-1.43679	0.034675	>1.4-fold change
Ahnak2	Uncharacterized protein	-1.4042347	0.005449	